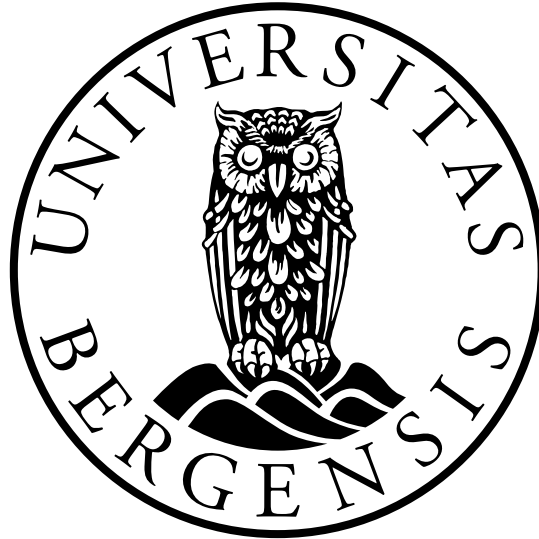# UNIVERSITY OF BERGEN

Department of Physics and Technology

Search for squarks in events with jets, hadronically decaying τ-lepton, and missing transverse momentum in the final state in proton-proton collision at $\sqrt{s} = 13$ TeV with the ATLAS detector

---

Master Thesis in Physics
by
Wai Kit Leung

September 1, 2021

i

Abstract

Signal regions have been designed for search of squarks in events with jets, at least one hadronically decaying τ-lepton, and missing transverse momentum in the final state. The analysis is based on the LHC Run 2 dataset at $\sqrt{s} = 13$ TeV with an integrated luminosity of 139 fb^{-1}. Two independent final states are considered, one with one τ-lepton in the final state and another with two or more τ-lepton in the final state. A simplified model of squark pair production is considered. An exclusion contour plot has been produced using only SR and with experimental systematic uncertainties. From the preliminary result of the exclusion contour plot, squark masses up to around 1700 GeV are expected to be excluded for low LSP masses at 95% confidence level, and LSP masses up to 800 GeV are expected to be excluded for squark masses around 1250 GeV.

Acknowledgement

Contents

1   Introduction

The Standard Model (SM) is a very successful model in particle physics. Over the last decades physicist have been trying to confront its prediction with experimental observation and so far, no evidence for physics beyond the Standard Model (BSM) have been found. However, there are hints that suggest it is not an ultimate theory, e.g indirect measurements testing the SM with high precision (sensitive to new physics through quantum loops) show tension with theory predictions, or cosmological observation indicates the existence of dark matter. A supersymmetric extension of SM is Supersymmetry (SUSY), and it introduces a superpartner (sparticles) for each particle in the Standard Model with the same quantum numbers, except for the spin that differs in half a unit (in $\bar{h}$). Supersymmetry provides solutions to some problems introduced by SM such as the Hierarchy problem (see Section 2) and the Lightest SUSY Particle (LSP) is a good candidate for the dark matter.

In The Minimal Supersymmetric Standard Model (MSSM) assuming R-parity, sparticles are produced in pairs and decay through cascades involving SM particles and other sparticles until the Lightest SUSY Particle (LSP), which is stable, is produced. In this thesis, signal regions (SRs) have been designed and studied for search of squarks produced via the strong interaction in events with jets, at least one hadronically decaying τ-lepton, and large missing transverse momentum from undetected LSP in the final state. The analysis is based on the full LHC Run 2 dataset of proton-proton collision at $\sqrt{s} = 13$ TeV with an integrated luminosity of 139 fb^{-1}, recorded with the ATLAS detector between 2015 and 2018. Two separate topology are studied, one with 1 τ-lepton in the final state and another with 2 or more τ-leptons in the final state. The SR optimization are done separately for these channels. A similar search with same final state objects is presented in (Aaboud et al., 2019), which considers simplified model of gluino pairs and a minimal model of Gauge-Mediated SUSY breaking (GMSB).

A brief overview of the Standard Model and the Minimal Supersymmetric Standard Model is given in Section 2. The Large Hadron Collider (LHC) and the ATLAS detector are described in Section 3. Section 4 presents how the different samples are simulated and how the objects used in this analysis are reconstructed. A description of the Asimov approximated discovery significance is given in Section 5, which is used to optimize the signal regions in Section 6. The signal regions are used to produce the exclusion contour plots in section 7. Finally, a summary and an outlook is discussed in Section 8.

2 Theory

2.1 The Standard Model

In this section, we will give brief descriptions of quantum field theory, gauge theories and the Brout–Englert–Higgs mechanism which constitute the standard model. The descriptions are mostly taken from (Mandl and Shaw, 2010). For more details, please read the reference. In the book the Einstein's notation for summation is used and will also be used here. Some notation used here may also differ from the book.

2.1.1 Quantum Field Theory

Before we discuss Quantum Field Theory, let us look at Lagrangian mechanics first. The action in Lagrangian mechanics is:

$$S = \int_{t_1}^{t_2} L(x_n(t), \dot{x}_n(t), t)dt \tag{2.1}$$

Where x_n is a generalised coordinate, $\dot{x}_n$ is the derivative of x_n with respect to t and L is the Lagrangian which is a function of x_n, $\dot{x}_n$ and t. If we vary $x(t)$ by $x(t) \rightarrow x(t) + \delta x(t)$ and keep variation at the end points fixed i.e $\delta x(t_1) = \delta x(t_2) = 0$, then by Hamiltion's principle the action is stationary i.e $\delta S = 0$. From (2.1) it gives us the equation of motion (e.o.m):

$$\frac{\partial L}{\partial x_n} - \frac{d}{dt}\frac{\partial L}{\partial \dot{x}_n} = 0 \tag{2.2}$$

Moving on to Lagrangian field theory is relative easy. We replace our set of generalised coordinates x_n with a set of fields $\phi_r(x^\mu)$ which is a function of our coordinates and t. We also replace L by the Lagrangian density $\mathcal{L}$ defined as

$$L = \int \mathcal{L}d^3x$$

Analogous to (2.1) the action is:

$$S = \int_\Omega \mathcal{L}(\phi_r(x^\mu), \partial_\mu \phi_r(x^\mu)) d^4 x \tag{2.3}$$

Similar to Lagrangian mechanics, we vary $\phi_r(x^\mu)$ by $\phi_r(x^\mu) \to \phi_r(x^\mu) + \delta\phi_r(x^\mu)$ and $\delta\phi_r(x^\mu) = 0$ at the boundary of Ω. By Hamilton's principle the action is stationary. Applying this to (2.3) gives us the Euler-Lagrange e.o.m:

$$\frac{\partial \mathcal{L}}{\partial \phi_r} - \partial_\mu \frac{\partial \mathcal{L}}{\partial(\partial_\mu \phi_r)} = 0 \tag{2.4}$$

An example is a Lagrangian with one real scalar field:

$$\mathcal{L} = \frac{1}{2}(\partial^\mu \phi)(\partial_\mu \phi) - \frac{1}{2}m^2\phi^2 \tag{2.5}$$

plugging this into (2.4) gives the Klein-Gordon field:

$$\partial_\mu \partial^\mu \phi + m^2 \phi = 0 \tag{2.6}$$

From Noether's theorem we know that continuous symmetry of action implies conservation of current. Consider the infinitesimal transformation:

$$\phi_r(x^\mu) \to \phi_r'(x^\mu) = \phi_r(x^\mu) + \epsilon\Delta\phi_r(x^\mu) \Rightarrow \mathcal{L} \to \mathcal{L} + \Delta\mathcal{L}$$

For symmetry transformation of the action, we get the conserved current j^μ:

$$j^\mu = \frac{\partial \mathcal{L}}{\partial(\partial_\mu \phi_r)}\Delta\phi_r - J^\mu \tag{2.7}$$

where $\partial_\mu J^\mu = \Delta\mathcal{L}$ and j^μ satisfies $\partial_\mu j^\mu = 0$.

Let us look at the Klein-Gordon field again (eq.(2.6)), and consider a large box of volume $V = L^3$. The general solution is superposition of planar

waves:

$$\phi(x) = \sum_{\vec{k}} \left[a(\vec{k}, t)e^{i\vec{k}\cdot\vec{x}} + a^*(\vec{k}, t)e^{-i\vec{k}\cdot\vec{x}} \right] \qquad (2.8)$$

where $\vec{k}$ is the momentum and is restricted as such:

$$k^i = \frac{2\pi}{L}n^i, n^i \in \mathbb{N}$$

If we plug (2.8) into (2.6) we get this equation:

$$\sum_{\vec{k}} \ddot{a}(\vec{k}, t) + \omega_k^2 a(\vec{k}, t) = 0 \qquad (2.9)$$

Which can be recognized as a sum of Harmonic Oscillators. We can quantize the field in analogy with Harmonic Oscillator. Now a and a^* become creation and annihilation operators $\hat{a}$ and $\hat{a}^\dagger$. The Klein-Gordon field becomes a field operator:

$$\hat{\phi}(x) = \sum_{\vec{k}} \left[\hat{a}(\vec{k})e^{-ikx} + \hat{a}^\dagger(\vec{k})e^{ikx} \right] \qquad (2.10)$$

The operators $\hat{a}$ and $\hat{a}^\dagger$ have analogous commutation relation with Harmonic Oscillators:

$$[\hat{a}(\vec{k}), \hat{a}^\dagger(\vec{k'})] = \delta_{\vec{k},\vec{k'}} \qquad (2.11)$$

Quantization of the complex Klein-Gordon field, Dirac field and photon field are done analogous to the real Klein-Gordon field.

2.1.2 Quantum Electrodynamics (QED)

For quantum Electrodynamics the form of interaction is well known from classical theory of Maxwell and Lorentz, but for our other strong and weak

forces, there is no classical theories to guide us. The way forward is to postulate forms of interaction and test their prediction against experiments. This is however not done blindly and is restricted by general theoretical and experimental requirements. Theoretically, we require the theory to be Lorentz invariant, local invariant and re-normalizable. It then remains to find Lagrangian densities which fit these requirements. For QED we introduce the free-fermion Lagrangian density:

$$\mathcal{L} = \bar{\psi}(x)(i\slashed{\partial} - m)\psi(x) \tag{2.12}$$

for which the e.o.m is the Dirac field. Here we used Feynman's slash notation which is defined as follows: $\slashed{\partial} \equiv \gamma^\mu \partial_\mu$ where γ^μ are the Dirac matrices. The Lagrangian is invariant under global phase transformation:

$$\psi \to e^{-iqe\epsilon}\psi$$
$$\bar{\psi} \to e^{-iqe\epsilon}\bar{\psi}$$

From (2.7) we find the conserved current:

$$j^\mu = qe\bar{\psi}\gamma^\mu\psi \tag{2.13}$$

Which gives us the conservation of charge:

$$Q = \int j^0 d^3x = qe \int \psi^\dagger \psi d^3x$$

This Lagrangian density is however, not invariant under local transformation

$$\psi \to e^{-iqe\epsilon(x)}\psi$$
$$\bar{\psi} \to e^{iqe\epsilon(x)}\bar{\psi}$$

We can regain our invariance by replacing the derivative ∂_μ by the covariant derivative $D_\mu = \partial_\mu + iqA_\mu(x)$.

$$\mathcal{L} = \bar{\psi}(x)(i\slashed{D} - m)\psi(x) \tag{2.14}$$

Which is invariant under the gauge transformation of the photon field $A_\mu(x)$:

$$A_\mu(x) \rightarrow A_\mu(x) + \partial_\mu \epsilon(x) \tag{2.15}$$

Looking closely at eq.(2.14), we can divide the Lagrangian into a free Lagrangian and an interaction Lagrangian:

$$\mathcal{L} = \bar{\psi}(x)(i\slashed{\partial} - m)\psi(x) + qe\bar{\psi}(x)\slashed{A}(x)\psi(x) = \mathcal{L}_0 + \mathcal{L}_I \tag{2.16}$$

We can see from this approach, interaction between fermions and photons are introduced.

2.1.3   Quantum Chromodynamics (QCD)

We can use the same approach as QED to find the form of interaction for the strong interaction. We start with the free quark Lagrangian density:

$$\mathcal{L} = \left[\bar{\psi}_b^f(x)(i\slashed{\partial} - m_f)\psi_b^f(x) + \bar{\psi}_r^f(x)(i\slashed{\partial} - m_f)\psi_r^f(x) + \bar{\psi}_g^f(x)(i\slashed{\partial} - m_f)\psi_g^f(x) \right] \tag{2.17}$$

where r, g, b denotes the colour charge of the quarks and $f = u, d, s, c, b, t$ denotes the flavour. We can combine the Dirac fields $\psi_{r,b,g}^f$ into a three component field:

$$\Psi^f = \begin{pmatrix} \psi_r^f \\ \psi_g^f \\ \psi_b^f \end{pmatrix}$$
$$\bar{\Psi}^f = \begin{pmatrix} \bar{\psi}_r^f & \bar{\psi}_g^f & \bar{\psi}_b^f \end{pmatrix} \tag{2.18}$$

(2.17) simplifies to:

$$\mathcal{L} = \bar{\Psi}^f(x)(i\slashed{\partial} - m_f)\psi^f(x) \tag{2.19}$$

6

The Lagrangian density is invariant under the global transformation:

$$\Psi^f(x) \rightarrow U(\alpha)\Psi^f(x) \equiv e^{i\alpha_i\lambda_i/2}\Psi^f(x)$$
$$\bar{\Psi}^f(x) \rightarrow \bar{\Psi}^f(x)U^\dagger(\alpha) \equiv \bar{\Psi}^f(x)e^{-i\alpha_i\lambda_i/2} \tag{2.20}$$

where α_i are eight arbitrary real numbers, $U(\alpha)$ comprise the SU(3) group where λ_i are the Gell-Mann matrices which are the generator for SU(3) group. The SU(3) group is Non-abelian in nature and the Gell-Mann matrices have a non-zero commutation relation:

$$[\frac{\lambda_i}{2}, \frac{\lambda_j}{2}] = if_{ijk}\frac{1}{2}\lambda_k \tag{2.21}$$

sum over repeated color indices k is understood here. The structure constant f_{ijk} is totally antisymmetric and is determined by looking at the matrices (see Mandl and Shaw (2010) page. 223). Conservation of current follows from invariance under the SU(3) transformation. If we do an infinitesimal transformation (2.20), it reduces to:

$$\Psi^f(x) \rightarrow (1 + i\alpha_i\lambda_i/2)\Psi^f(x)$$
$$\bar{\Psi}^f(x) \rightarrow \bar{\Psi}^f(x)(1 - i\alpha_i\lambda_i/2) \tag{2.22}$$

If we apply (2.7) together with (2.22) and (2.19), we get 8 conserved currents:

$$j_i^\mu(x) = \frac{1}{2}\bar{\Psi}^f(x)\gamma^\mu\lambda_i\Psi^f(x) \tag{2.23}$$

The corresponding conserved charges are:

$$Q_i = \int j_i^0(x)d^3x = \frac{1}{2}\int \Psi^{f\dagger}(x)\lambda_i\Psi^f(x)d^3x \tag{2.24}$$

Which are just the field-theoretic realization of the color charges. The next step is to generalize the global SU(3) transformation to local transformation. The approach is analogous to QED. First, we replace our global

transformation with local ones:

$$\begin{aligned}
\Psi^f(x) &\to e^{ig_s\omega_i\lambda_i/2}\Psi^f(x) \\
\bar{\Psi}^f(x) &\to \bar{\Psi}^f(x)e^{-ig_s\omega_i\lambda_i/2}
\end{aligned} \tag{2.25}$$

Here g_s is our coupling constant and ω_i $(j = 1, 2, ..., 8)$ are real differentiable functions. As in QED, to re-obtain our invariance, we replace the derivative with the covariant derivative:

$$D_\mu = \partial_\mu + ig_s\lambda_i A_i^\mu(x)/2 \tag{2.26}$$

Our Lagrangian density then goes over to:

$$\mathcal{L} = \bar{\Psi}^f(x)(i\slashed{D} - m_f)\psi^f(x) = \bar{\Psi}^f(x)(i\slashed{\partial} - m_f)\psi^f(x) + -\tfrac{1}{2}g_s\bar{\Psi}^f(x)\gamma^\mu\lambda_i\psi^f(x)A_i^\mu(x)$$
$$= \mathcal{L}_0 + \mathcal{L}_I \tag{2.27}$$

Here $A_i^\mu(x)$ are eight real gauge fields called gluon fields, as there are eight conserved charges and arbitrary functions $\omega_i(x)$ in the local transformation. Quark-gluon interactions are introduced in $\mathcal{L}_I$. The matrices γ_i are not all diagonal and hence, this interaction can annihilate quarks of one color and create one with another. By color conservation, the gluons must have non-zero charges. This is in contrast to QED, where the photons have zero electric charge. For the modified Lagrangian density to be invariant under SU(3) transformation, the transformation must be coupled to the transformation of $A_i^\mu(x)$ which are chosen in such a way so that the covariant derivative (2.26) transforms the same way as the fields $\psi^f(x)$ themselves:

$$D^\mu\psi^f(x) \to e^{ig_s\omega_i\lambda_i/2}D^\mu\psi^f(x) \tag{2.28}$$

One can show that the infinitesimal transformation of $A_i^\mu(x)$ is given by:

$$A_i^\mu(x) \to A_i^\mu(x) - \partial^\mu\omega_i(x) - g_s f_{ijk}\omega_j(x)A_k^\mu(x) \tag{2.29}$$

This is very similar to transformation of photons except for the last term: $-g_s f_{ijk}\omega_j(x)A_k^\mu(x)$, which is a result from non-abelian nature of the SU(3)

group. We shall see later that this results in the introduction of gluon self interaction.

The Lagrangian density (2.19) describes the quark field and their interaction with the gluon fields. For a complete Lagrangian density, we include a term which describe gluons without any quarks present. We can use a similar term to that of the free photon:

$$-\frac{1}{4}F_{i\mu\nu}(x)F_i^{\mu\nu}(x) \tag{2.30}$$

where

$$F_i^{\mu\nu}(x) \equiv \partial^\nu A_i^\mu(x) - \partial^\mu A_i^\nu(x) \tag{2.31}$$

But, this expression is not invariant under gauge transformation, on the account of the term $-g_s f_{ijk}\omega_j(x)A_k^\mu(x)$ in (2.29). We introduce additional terms in order to regain our invariance. $F_i^{\mu\nu}(x)$ is then replaced by

$$G_i^{\mu\nu}(x) \equiv F_i^{\mu\nu}(x) + g_s f_{ijk}A_j^\mu(x)A_k^\nu(x) \tag{2.32}$$

which gives us the gauge invariant expression:

$$\mathcal{L}_G = -\frac{1}{4}G_{i\mu\nu}(x)G_i^{\mu\nu}(x) \tag{2.33}$$

The complete Lagrangian density for QCD is obtained by combining (2.27) and (2.33):

$$\mathcal{L} = \bar{\Psi}^f(x)(i\slashed{D} - m_f)\psi^f(x) - \frac{1}{4}G_{i\mu\nu}(x)G_i^{\mu\nu}(x) \tag{2.34}$$

Let us take a closer look at (2.33). We expand the equation using (2.32):

$$\mathcal{L}_G = -\frac{1}{4}F_{i\mu\nu}(x)F_i^{\mu\nu}(x) + g_s f_{ijk}A_{i\mu}(x)A_{j\nu}(x)\partial^\mu A_k^\nu(x) \\ -\frac{1}{4}g_s^2 f_{ijk}f_{ilm}A_j^\mu(x)A_k^\nu(x)A_{l\mu}(x)A_{m\nu}(x) \tag{2.35}$$

The first term is the Lagrangian density for eight non-interacting massless spin 1 gluons. The second and third terms are the result of the additional term in (2.32) and introduce interactions between gluon fields themselves. These interactions arise because the gluons, which transmit interaction between color charges, do not have non-zero color charges. This is in contrast to QED, where the photons have zero electric charge and do not self-interact. Another property of QCD is that the interaction strength of quark-gluon interactions is independent from the quark flavour.

2.1.4 Gauge Theory of Weak Interactions

In analogy to QED, we can formulate a gauge theory of weak interactions. A unique property of the weak interactions is that it only involves left-handed lepton fields. This is corroborated by experiment results. The left- and right-handed lepton fields are defined by:

$$
\begin{aligned}
\psi^L(x) &= P_L \psi(x) \\
\psi^R(x) &= P_R \psi(x)
\end{aligned}
\tag{2.36}
$$

where P_L and P_R are the chiral projection operators:

$$
\begin{aligned}
P_L &= \tfrac{1}{2}(1 - \gamma^5) \\
P_R &= \tfrac{1}{2}(1 + \gamma^5)
\end{aligned}
\tag{2.37}
$$

Here, γ^5 is recognized as $\gamma^5 \equiv i\gamma^0\gamma^1\gamma^2\gamma^3$. The Lagrangian density is:

$$
\mathcal{L} = i \left[\bar{\psi}_l^L(x)\slashed{\partial}\psi_l^L(x) + \bar{\psi}_{\nu l}^L(x)\slashed{\partial}\psi_{\nu l}^L(x) + \bar{\psi}_l^R(x)\slashed{\partial}\psi_l^R(x) + \bar{\psi}_{\nu l}^R(x)\slashed{\partial}\psi_{\nu l}^R(x) \right]
\tag{2.38}
$$

where l corresponds to leptons νl corresponds to neutrino leptons and sum over all different leptons is understood. Note that unlike QED and QCD, the terms with masses are not included, as those terms will break symmetry. For now, we will move forward assuming the leptons are massless, and in section 2.1.5 we will re-introduce the mass terms back into the Lagrangian density. To simplify (2.38) we can combine the left-handed fields into a two-

component field:

$$\Psi_l^L(x) = \begin{pmatrix} \psi_l^L(x) \\ \psi_{\nu l}^L(x) \end{pmatrix}$$
$$\bar{\Psi}_l^L(x) = \left(\bar{\psi}_l^L(x), \bar{\psi}_{\nu l}^L(x) \right)$$

(2.39)

In terms of these fields, (2.38) becomes:

$$\mathcal{L} = i \left[\bar{\Psi}_l^L(x)\slashed{\partial}\Psi_l^L(x) + \bar{\psi}_l^R(x)\slashed{\partial}\psi_l^R(x) + \bar{\psi}_{\nu l}^R(x)\slashed{\partial}\psi_{\nu l}^R(x) \right]$$

(2.40)

We now introduce the SU(2) global transformations:

$$\Psi_l^L(x) \to U(\alpha)\Psi_l^L(x) \equiv e^{i\alpha_i\sigma_i/2}\Psi_l^L(x)$$
$$\bar{\Psi}_l^L(x) \to \bar{\Psi}_l^L(x)U^\dagger(\alpha) \equiv \bar{\Psi}_l^L(x)e^{-i\alpha_i\sigma_i/2}$$

(2.41)

which leaves the term $\bar{\Psi}_l^L(x)\slashed{\partial}\Psi_l^L(x)$ in (2.40) invariant. σ_i are the generators of the SU(2) group which are just the Pauli spin matrices. The matrices have a non-zero commutation relation:

$$[\sigma_i, \sigma_j] = 2i\epsilon_{ijk}\omega_k$$

(2.42)

here, ϵ_{ijk} is the completely antisymmetric tensor and summation over the indices ($k = 1, 2, 3$) is implied. Only left-handed fields have been considered. Now, we define the right-handed fields to be invariant under any SU(2) transformations:

$$\Psi_l^R(x) \to \Psi_l^R(x), \quad \Psi_{\nu l}^R(x) \to \Psi_{\nu l}^R(x)$$
$$\bar{\Psi}_l^R(x) \to \bar{\Psi}_l^R(x), \quad \bar{\Psi}_{\nu l}^R(x) \to \bar{\Psi}_{\nu l}^R(x)$$

(2.43)

The transformations (2.41) and (2.43) leaves the Lagrangian density (2.40) invariant. We now move on to infinitesimal transformations, which reduces (2.41) to:

$$\Psi_l^L(x) \to (1 + i\alpha_i\sigma_i/2)\Psi_l^L(x)$$
$$\bar{\Psi}_l^L(x) \to \bar{\Psi}_l^L(x)(1 - i\alpha_i\sigma_i/2)$$

(2.44)

11

We apply (2.7), leading to three conserved currents:

$$j_i^\mu(x) = \frac{1}{2}\bar{\Psi}_l^L(x)\gamma^\mu\sigma_i\Psi_i^L(x) \tag{2.45}$$

with the corresponding conserved weak isospin charges:

$$I_i^W(x) = \int j_i^0(x)d^3x = \frac{1}{2}\int \Psi_l^{L\dagger}(x)\sigma_i\Psi_i^L(x)d^3x \tag{2.46}$$

$j_1^\mu(x)$ and $j_2^\mu(x)$ are the leptonic currents, but $j_3^\mu(x)$ couples together either electrically neutral leptons or electrically charged leptons:

$$j_3^\mu(x) = -\frac{1}{2}\left[\bar{\psi}_{\nu l}^L(x)\gamma^\mu\psi_{\nu l}^L(x) - \bar{\psi}_l^L(x)\gamma^\mu\psi_l^L(x)\right] \tag{2.47}$$

The last term of the right-hand side of (2.47) can be recognized as a part of the electromagnetic current (2.13). This indicates that the weak and electromagnetic processes are interconnected. We can define a hypercharge current:

$$J_Y^\mu(x) = -\frac{1}{2}\bar{\Psi}_l^L(x)\gamma^\mu\Psi_i^L(x) - \bar{\psi}_l^R(x)\gamma^\mu\psi_l^R(x) \tag{2.48}$$

The corresponding charge:

$$Y = \int J_Y^0(x)d^3x = Q/e - I_3^W \tag{2.49}$$

From (2.46) the hypercharge has different values depending on the chirality of the leptons and on its electric charge. For left-handed l^- and ν_l leptons, Y has the value $-\frac{1}{2}$, and for right-handed l^- and ν_l leptons it has the values -1 and 0 respectively. We can then introduce a U(1) global phase transformation:

$$\psi(x) \to e^{i\beta Y}\psi(x), \quad \bar{\psi}(x) \to \bar{\psi}(x)e^{-i\beta Y} \tag{2.50}$$

where β is an arbitrary real number. Next, we generalize the SU(2) and U(1) transformations from global to local transformations. We start with SU(2). The global transformations are replaced by local transformations:

$$
\begin{aligned}
\Psi_l^L(x) &\to e^{ig\sigma_i\omega_i(x)/2}\Psi_l^L(x) \\
\bar{\Psi}_l^L(x) &\to \bar{\Psi}_l^L(x)e^{-ig\sigma_i\omega_i(x)/2} \\
\psi_l^R(x) \to \psi_l^R(x), &\qquad \psi_{\nu l}^R(x) \to \psi_{\nu l}^R(x) \\
\bar{\psi}_l^R(x) \to \bar{\psi}_l^R(x), &\qquad \bar{\psi}_{\nu l}^R(x) \to \bar{\psi}_{\nu l}^R(x)
\end{aligned}
\tag{2.51}
$$

where $\omega_i(x)$, $i = 1, 2, 3$ are three arbitrary real differentiable functions of x, and g is the weak coupling constant. Our Lagrangian density from (2.40) is not invariant under these transformation. Similar to QED, we replace the ordinary derivative with the new covariant derivative:

$$
\partial^\mu \to D^\mu = \partial^\mu + ig\omega_i W_i^\mu(x)/2
\tag{2.52}
$$

$\mathcal{L}$ goes into:

$$
\mathcal{L} = i\left[\bar{\Psi}_l^L(x)\slashed{D}\Psi_l^L(x) + \bar{\psi}_l^R(x)\slashed{\partial}\psi_l^R(x) + \bar{\psi}_{\nu l}^R(x)\slashed{\partial}\psi_{\nu l}^R(x)\right]
\tag{2.53}
$$

In (2.52) we introduced three gauge fields W_i^μ. We can find the transformation law for our gauge fields analogous to (2.29):

$$
W_i^\mu(x) \to W_i^\mu(x) - \partial^\mu\omega_i(x) - g\epsilon_{ijk}\omega_j(x)W_k^\mu(x)
\tag{2.54}
$$

Moving on to U(1) transformation, the corresponding local transformations are:

$$
\psi(x) \to e^{ig'Yf(x)}\psi(x), \quad \bar{\psi}(x) \to \bar{\psi}(x)e^{-ig'Yf(x)}
\tag{2.55}
$$

where g' is a real number, and f(x) is an arbitrary real differential function. Y is the hypercharge from (2.49). Again, we obtain local invariance by replacing the derivative with covariant derivative:

$$
\partial^\mu \to D^\mu = \partial^\mu + ig'Y B^\mu(x)/2
\tag{2.56}
$$

The gauge field $B^\mu(x)$ is introduced here and transforms like:

$$B^\mu(x) \to B^\mu - \partial^\mu f(x) \tag{2.57}$$

If we simultaneously make both replacement (2.52) and (2.56) in (2.40), we get the leptonic Lagrangian density:

$$\mathcal{L}^L = i\left[\bar{\Psi}_l^L(x)\slashed{D}\Psi_l^L(x) + \bar{\psi}_l^R(x)\slashed{D}\psi_l^R(x) + \bar{\psi}_{\nu l}^R(x)\slashed{D}\psi_{\nu l}^R(x)\right] \tag{2.58}$$

where the derivatives are understood as:

$$\begin{aligned}
D^\mu\Psi_l^L(x) &= [\partial^\mu ig\omega_i W_i^\mu(x)/2 - ig'B^\mu(x)/2]\Psi_l^L(x) \\
D^\mu\psi_l^R(x) &= [\partial^\mu - ig'B^\mu(x)]\psi_l^R(x) \\
D^\mu\psi_{\nu l}^R(x) &= \partial^\mu\psi_{\nu l}^R(x)
\end{aligned} \tag{2.59}$$

If we define the fields $W_i^\mu(x)$ to be gauge invariant under U(1) transformations, and $B^\mu(x)$ to be invariant under SU(2) gauge transformations. The leptonic Lagrangian density from (2.58) is then invariant under SU(2) and U(1) transformations.

We can split (2.58) into a free Lagrangian and a interaction Lagrangian:

$$\mathcal{L} = \mathcal{L}_0 + \mathcal{L}_I \tag{2.60}$$

where $\mathcal{L}_I$ is given by:

$$\mathcal{L}_I = -gj_i^\mu(x)W_{i\mu}(x) - g'J_Y^\mu(x)B_\mu(x) \tag{2.61}$$

which represents the interaction of the weak isospin currents and the weak hypercharge current, with the gauge fields $W_{i\mu}(x)$ and $B_\mu(x)$. We can write the weak isospin current $j_1^\mu(x)$ and $j_2^\mu(x)$ in terms of the charged leptonic currents $j^\mu(x)$ and $j^{\mu\dagger}(x)$:

$$\begin{aligned}
j^\mu(x) &= 2\left[j_1^\mu(x) - ij_2^\mu(x)\right] \\
j^{\mu\dagger}(x) &= 2\left[j_1^\mu(x) + ij_2^\mu(x)\right]
\end{aligned} \tag{2.62}$$

We also introduce the non-Hermitian gauge field:

$$W_\mu(x) = \frac{1}{\sqrt{2}} \left[W_{1\mu}(x) - iW_{2\mu}(x) \right] \tag{2.63}$$

The first two terms in (2.61) becomes:

$$-g \sum_{i=1}^{2} j_i^\mu(x) W_{i\mu}(x) = \frac{-g}{2\sqrt{2}} \left[j^{\mu\dagger}(x) W_\mu(x) + j^\mu(x) W_\mu^\dagger(x) \right] \tag{2.64}$$

In the two remaining two terms, we write $W_{3\mu}(x)$ and $B_\mu(x)$ as a linear combination of two different Hermitian fields $A_\mu(x)$ and $Z_\mu(x)$, defined by:

$$\begin{aligned} W_{3\mu}(x) &= cos\theta_W Z_\mu(x) + sin\theta_W A_\mu(x) \\ B_\mu(x) &= -sin\theta_W Z_\mu(x) + cos\theta_W A_\mu(x) \end{aligned} \tag{2.65}$$

where the θ_W is the Weingberg angle and determines the mixture of $A_\mu(x)$ and $Z_\mu(x)$ in $W_{3\mu}(x)$ and $B_\mu(x)$. The value of this angle was experimentally found to be $sin^2\theta_W = 0.23122 \pm 0.00015$. From our hypercharge current:

$$J_Y^\mu = S^\mu(x)/e - J_3^\mu(x) \tag{2.66}$$

where $S^\mu(x)$ is the electromagnetic current from (2.13) and together with (2.65), we obtain:

$$\begin{aligned} &-gj_3^\mu(x) W_{3\mu}(x) - g' J_Y^\mu B_\mu(x) \\ = &-\frac{g'}{e} s^\mu(x) \left[-sin\theta_W Z_\mu(x) + cos\theta_W A_\mu(x) \right] \\ &-j_3^\mu(x) \left\{ g \left[cos\theta_W Z_\mu(x) + sin\theta_W A_\mu(x) \right] \right. \\ &\left. -g' \left[-sin\theta_W Z_\mu(x) + cos\theta_W A_\mu(x) \right] \right\} \end{aligned} \tag{2.67}$$

If we demand that the gauge field $A_\mu(x)$ is the electromagnetic field and is coupled to charges in the usual way, the coefficient of $j_3^\mu(x) A_\mu(x)$ must vanish and that of $s^\mu(x) A_\mu(x)$ must be -1. We require:

$$gsin\theta_W = g'cos\theta_W = e \tag{2.68}$$

15

We can substitute (2.64) and (2.67) in (2.61) and eliminate g' by (2.68).We then obtain the final expression for the interaction Lagrangian density:

$$
\begin{aligned}
\mathcal{L}^L = -s^\mu(x)A_\mu(x) &- \tfrac{-g}{2\sqrt{2}}\left[j^{\mu\dagger}(x)W_\mu(x) + j^\mu(x)W_\mu^\dagger(x)\right] \\
&- \tfrac{g}{cos\theta_W}\left[j_3^\mu(x)sin^2\theta_W s^\mu(x)/e\right]Z_\mu(x)
\end{aligned}
\tag{2.69}
$$

The first term in (2.69) is the familiar interaction of QED. The second term is interaction with the $W^\pm$ vector bosons. The last term represents a neutral current, and the gauge field $Z_\mu(x)$ corresponds to the neutral vector boson Z^0.

Until now, we only described the the free lepton and their interaction with the gauge fields. The complete Lagrangian density must also contain terms which describes gauge bosons with no leptons present. As with the leptons, we shall assume the gauge bosons have zero masses. How to include massive gauge bosons will be discussed in the next section. In analogy with QED, a SU(2) × U(1) gauge-invariant Lagrangian density for $B^\mu(x)$ is given by:

$$
-\frac{1}{4}B_{\mu\nu}(x)B^{\mu\nu}(x)
\tag{2.70}
$$

where

$$
B^{\mu\nu}(x) \equiv \partial^\nu B^\mu(x) - \partial^\mu B^\nu(x)
\tag{2.71}
$$

As with QCD, simply making a Lagrangian density in analogy to (2.70) for the $W_i^\mu(x)$ fields is not enough to make it invariant. Because of the non-Abelian nature of the SU(2) transformation we introduce additional interaction terms to gain invariance. We define $G_i^{\mu\nu}$:

$$
G_i^{\mu\nu}(x) \equiv F_i^{\mu\nu}(x) + g\epsilon_{ijk}W_j^\mu(x)W_k^\nu(x)
\tag{2.72}
$$

where

$$
F_i^{\mu\nu}(x) \equiv \partial^\nu F_i^\mu(x) - \partial^\mu F_i^\nu(x)
\tag{2.73}
$$

16

The SU(2) gauge-invariant expression is then:

$$-\frac{1}{4}G_{i\mu\nu}(x)G_i^{\mu\nu}(x) \tag{2.74}$$

Combining the expression from (2.70) and (2.74), and substituting (2.72), we get the complete SU(2) × U(1) gauge-invariant Lagrangian density for gauge bosons:

$$\begin{aligned}
\mathcal{L}^B = &-\tfrac{1}{4}B_{\mu\nu}(x)B^{\mu\nu}(x) - \tfrac{1}{4}F_{i\mu\nu}(x)F_i^{\mu\nu}(x) \\
&+g\epsilon_{ijk}W_{i\mu}(x)W_{j\nu}(x)\partial^\mu W_k^\nu(x) \\
&-\tfrac{1}{4}g^2\epsilon_{ijk}\epsilon_{ilm}W_j^\mu(x)W_k^\nu(x)W_{i\mu}(x)W_{m\nu}(x)
\end{aligned} \tag{2.75}$$

The first two terms represent the Lagrangian density of free gauge fields. The last two terms describes interaction amongst the gauge bosons themselves. In perturbation theory the terms corresponds to vertices with three- or four lines. The interactions arise because the $W_i^\mu(x)$ fields, which transmit the interactions between the weak isospin currents, carry isospin charge themselves.

2.1.5   The Brout–Englert–Higgs mechanism

In previous chapter we assumed that the leptons and gauge bosons are massless. In this section we shall see that the mass terms in Lagrangian density by the Brout-Englert-Higgs mechanism. But, first we begin with the Goldstone model and spontaneous symmetry breaking.

Spontaneous symmetry breaking briefly explained, is when we have symmetry in all states, but the ground state. A example of such asymmetric ground state is Ferromagnetism. In field theory the ground state is the vacuum state. The quantity for such a state is the vacuum expectation value (VEV) of quantized field. If we assume spontaneously broken symmetry and the vacuum state is invariant under Lorentz transformations, and under translation, then the field must be a scalar field and its vacuum expectation value constant:

$$\langle 0| \phi(x) |0\rangle = c \tag{2.76}$$

The vacuum expectation value of any spinor fields $\psi(x)$ and vector field $V^\mu(x)$ must vanish:

$$\langle 0 | \psi(x) | 0 \rangle = 0, \quad \langle 0 | V^\mu(x) | 0 \rangle = 0 \tag{2.77}$$

The simplest example of a field theory exhibiting spontaneous symmetry breaking is the Goldstone model. Its Lagrangian density is:

$$\mathcal{L} = (\partial^\mu \phi^*(x)) \, (\partial_\mu \phi(x)) - u^2 \, |\phi(x)|^2 - \lambda \, |\phi(x)|^4 \tag{2.78}$$

where

$$\phi(x) = \frac{1}{\sqrt{2}} \, [\phi_1(x) + i\phi_2(x)] \tag{2.79}$$

is a complex scalar field, and u^2 and λ are arbitrary real parameters. This Lagrangian density is invariant under global U(1) phase transformation given by:

$$\phi(x) \to \phi(x)e^{i\alpha}, \quad \phi^*(x) \to \phi^*(x)e^{-i\alpha} \tag{2.80}$$

In the ground state $\phi(x)$ must be a constant, and we also require $\lambda > 0$ for the energy of the field to be bounded from below. The constant $\phi(x) = \phi_0$ at the vacuum state can be found by minimizing the potential term:

$$u^2 \, |\phi(x)|^2 - \lambda \, |\phi(x)|^4 \tag{2.81}$$

with respect to ϕ_0. If we assume that $u^2 < 0$ the potential term (2.81) has a local minimum at $\phi_0 = 0$ and a circle of absolute minima at:

$$\phi_0 = \left(\frac{-u^2}{2\lambda} \right)^{1/2} e^{i\theta}, \quad 0 \le \theta \le 2\pi \tag{2.82}$$

The phase angle θ defines a direction in the complex ϕ-plane. The vacuum state is not unique in this case, but since it should only exist only one vacuum

18

state, we choose one particular directon θ to represent the vacuum. The simplest case is when $\theta = 0$:

$$\phi_0 = \left(\frac{-u^2}{2\lambda}\right)^{1/2} = \left(\frac{1}{\sqrt{2}}v\right) \tag{2.83}$$

Eq.(2.83) is no longer invariant under the transformations (2.80), as the transformations will just point θ in an other direction. Thus, we have spontaneously symmetry breaking. We can rewrite $\phi(x)$ in (2.78) in terms of two Klein-Gordon fields $\sigma(x)$ and $\eta(x)$:

$$\phi(x) = \frac{1}{\sqrt{2}}\left[v + \sigma(x) + i\eta(x)\right] \tag{2.84}$$

The $\sigma(x)$ field corresponds to a massive neutral spin-0 particle, while $\eta(x)$ corresponds to a so-called Nambu-Goldstone boson. Since, by definition, there are no particles present in the vacuum, the VEV of (2.84) is:

$$\langle 0| \phi(x) |0\rangle = \frac{1}{\sqrt{2}}v \tag{2.85}$$

Which is a non-zero constant and a condition for spontaneous symmetry breaking from (2.76).

We now move on to introducing a Lagrangian density which we break for SU(2) × U(1) symmetry. This includes introducing a Higgs field, i.e a scalar field with non-vanishing VEV which is not invariant under our gauge transformations. For SU(2) symmetry, we need a field with multiple components and non-zero isospin. The simplest case is a weak isospin doublet:

$$\Phi(x) = \begin{pmatrix} \phi_a(x) \\ \phi_b(x) \end{pmatrix} \tag{2.86}$$

The transformation laws for $\Phi(x)$ are the same as for $\Psi_l^L(x)$ given in (2.41) and (2.50). Analogously the SU(2) local transformations are:

$$\begin{aligned} \Phi(x) &\rightarrow e^{ig\sigma_i\omega_i(x)/2}\Phi(x) \\ \Phi^\dagger(x) &\rightarrow \Phi^\dagger(x)e^{-ig\sigma_i\omega_i(x)/2} \end{aligned} \tag{2.87}$$

and U(1) local transformations are:

$$\begin{aligned}\Phi(x) &\rightarrow e^{ig'Yf(x)}\Phi(x) \\ \Phi^{\dagger}(x) &\rightarrow \Phi^{\dagger}(x)e^{-ig'Yf(x)}\end{aligned} \tag{2.88}$$

As in the previous section, to obtain local symmetry, we replace the common derivative with our covariant derivative:

$$D^{\mu} = \partial^{\mu} + ig\sigma_i W_i^{\mu}(x)/2 + ig'YB^{\mu}(x) \tag{2.89}$$

The Lagrangian density for the Higgs model, which is local gauge invariant under SU(2) × U(1) transformations is similar to (2.78):

$$\mathcal{L}^H = (D^{\mu}\Phi(x))^{\dagger}(D_{\mu}\Phi(x)) - u^2\Phi^{\dagger}(x)\Phi(x) - \lambda\left[\Phi^{\dagger}(x)\Phi(x)\right]^2 \tag{2.90}$$

Analogous to the Goldstone model, if we require $\lambda > 0$ and $u^2 = 0$, the classical energy density is a minimum for a constant Higgs field:

$$\Phi_0 = \begin{pmatrix}\phi_a^0 \\ \phi_b^0\end{pmatrix} \tag{2.91}$$

with

$$\Phi_0^{\dagger}\Phi_0 = \left|\phi_a^0\right|^2 + \left|\phi_b^0\right|^2 = \frac{-u^2}{2\lambda} \tag{2.92}$$

Choosing a particular value Φ_0 leads to spontaneous symmetry breaking. Without loss of generality, we can choose:

$$\Phi_0 = \begin{pmatrix}0 \\ v/\sqrt{2}\end{pmatrix} \tag{2.93}$$

where

$$v = \left(\frac{-u^2}{\lambda} \right)^{1/2} \tag{2.94}$$

The photons are massless particles, thus we do not want to spontaneous break symmetry for $U(1)_{EM}$ transformations. The particle corresponding to the Higgs field must have null electric charge. From (2.49) we find that the hypercharge $Y = -I_3^W$. We find the value of I_3^W by using (2.46) with the Higgs field (2.86). The hypercharge is then found to be: $Y = -\frac{1}{2}$. The covariant derivative becomes:

$$D^\mu = \partial^\mu + ig\sigma_i W_i^\mu(x)/2 + ig' B^\mu(x)/2 \tag{2.95}$$

An arbitrary Higgs field can be parametrized in analogy to (2.84):

$$\Phi(x) = \frac{1}{\sqrt{2}} \begin{pmatrix} \eta_1(x) + i\eta_2(x) \\ v + H(x) + i\eta_3(x) \end{pmatrix} \tag{2.96}$$

Here, the field $H(x)$ corresponds to the Higgs particle, and the three fields η_i, $i = 1, 2, 3$ are the Nambu-Goldstone bosons, which will cause non-physical properties in the Lagrangian density from (2.90) (more details in the reference by Mandl and Shaw (2010)). To get rid of these un-physical bosons, we employ a special gauge called the unitary gauge. This gauge transforms the field $\Phi(x)$, in a similar way to (2.87), into simply:

$$\Phi(x) = \frac{1}{\sqrt{2}} \begin{pmatrix} 0 \\ v + H(x) \end{pmatrix} \tag{2.97}$$

Substituting (2.65) in (2.90) to express the gauge fields in terms of $W^\pm$ and Z_0 bosons ($A^\mu(x)$ vanishes because the $\Phi(x)$ field is neutral), and using (2.95) for the covariant derivative, the kinetic term $(D^\mu\Phi(x))^\dagger (D_\mu\Phi(x))$ in (2.90) becomes:

$$\mathcal{L}_k^H = \frac{1}{2} (\partial_\mu H(x)) (\partial^\mu H(x)) + \frac{1}{4} g^2 W_\mu^+ W^{-\mu} (v + H(x))^2 + \frac{1}{8} g'^2 Z_\mu Z^\mu (v + H(x))^2 \tag{2.98}$$

21

where the Weinberg angle θ_W has been neglected. The terms with v^2 are recognized as the $W^{\pm}$ and Z boson mass terms:

$$
M_W^2 W_\mu^+ W^{-\mu} + \tfrac{1}{2} M_Z^2 Z_\mu Z^\mu, \\
M_W^2 = \tfrac{1}{4} g^2 v^2 \\
M_Z^2 = \tfrac{1}{4} \tfrac{v}{2} \sqrt{g^2 + g'^2} = M_W / cos(\theta_W)
\tag{2.99}
$$

The potential term $u^2 \Phi^\dagger(x) \Phi(x) - \lambda \left[\Phi^\dagger(x) \Phi(x) \right]^2$ in (2.90) is:

$$
\mathcal{L}_p^H = \frac{1}{2} \left(-2\mu^2 \right) H^2(x) - \frac{1}{4} \mu^2 v^2 \left[-1 + \frac{4H^3(x)}{v^3} + \frac{H^4(x)}{v^4} \right]
\tag{2.100}
$$

Together with the first term from (2.98) describes the Higgs boson:

$$
\frac{1}{2} \left(\partial_\mu H(x) \right) \left(\partial^\mu H(x) \right) - \frac{1}{2} \left(-2\mu^2 \right) H^2(x) + \frac{1}{4} \mu^2 v^2 \left[-1 + \frac{4H^3(x)}{v^3} + \frac{H^4(x)}{v^4} \right]
\tag{2.101}
$$

The second term in (2.101) give us the Higgs boson's mass $M_H = \sqrt{-2\mu^2}$. The cubic and quartic terms in $H(x)$ correspond to Higgs boson self-interaction, which in perturbation theory gives vertices with three or four lines. The rest of the terms in (2.98) corresponds to interactions between the Higgs field and the other gauge fields:

$$
\left(\frac{1}{4} g^2 W_\mu^+ W^{-\mu} + \frac{1}{8} g'^2 Z_\mu Z^\mu \right) \left(H^2(x) + 2v H(x) \right)
\tag{2.102}
$$

We have now achieved to introduce mass terms in a Lagrangian density which is SU(2) × U(1) gauge-invariant and re-normalizable. What remains now is to introduce mass to our fermions. For leptons, this is accomplished by Yukawa interaction between lepton and ϕ fields that is SU(2) × U(1) gauge-invariant and re-normalizable:

$$
\mathcal{L}^{LH} = -Y_{jl}^l \bar{\Psi}_l^L(x) \Phi(x) e_j^R(x) - Y_{jl}^{\nu_l} \bar{\Psi}_l^L(x) \tilde{\Phi}(x) \nu_{lj}^R(x) + h.c
\tag{2.103}
$$

where Y_{jl}^l and $Y_{jl}^{\nu l}$ are 3×3 Yukawa matrices, which its elements consist of arbitrary coupling constants. $Y_{jl}^{\nu l}$ is not a diagonal matrix and will introduce neutrino mixing. $\tilde{\Phi}(x)$ is defined by:

$$\tilde{\Phi}(x) = -i \left[\Phi^\dagger \sigma_2 \right]^T \tag{2.104}$$

$e_j^R(x)$ and $\nu_{lj}^R(x)$ are three component field which includes all three generations indexed by j:

$$e_j(x) = \begin{pmatrix} e^R(x) \\ \mu^R(x) \\ \tau^R(x) \end{pmatrix}$$
$$\nu_{lj}(x) = \begin{pmatrix} \nu_e^R(x) \\ \nu_\mu^R(x) \\ \nu_\tau^R(x) \end{pmatrix} \tag{2.105}$$

Using the unitary gauge (2.97),(2.103) introduces the mass terms and interaction terms:

$$-y_l \frac{v}{\sqrt{2}} \bar{\psi}_l \psi_l - y_l \frac{v}{\sqrt{2}} H \bar{\psi}_l \psi_l,$$
$$m_l = -y_l \frac{v}{\sqrt{2}} \tag{2.106}$$

where y_l are the diagonal elements of Y^l matrix. The second term in (2.106) corresponds to interaction between the Higgs boson and leptons.

2.1.6   The Standard Model

If we combine the Lagrangian densities from the last two sections, we get the standard electroweak theory. What we lack now is a Lagrangian density that describes the weak interaction with quarks. We need a Lagrangian density that is SU(3) $\times$ SU(2) $\times$ U(1) gauge-invariant:

$$\mathcal{L}^q = i \left[\bar{q}_L^f(x) \not{D} q_L^f(x) + \bar{q}_{uR}^f(x) \not{D} q_{uR}^f(x) + \bar{q}_{dR}^f(x) \not{D} q_{dR}^f(x) \right] \tag{2.107}$$

where $q^f(x)$ is a weak doublet for quarks:

$$q^f(x) = \begin{pmatrix} q_u^f(x) \\ q_d^f(x) \end{pmatrix} \tag{2.108}$$

$q_{uR}^f(x)$ and $q_{dR}^f(x)$ are the right-handed three component Dirac fields from (2.18). The covariant derivatives corresponds to:

$$\begin{aligned}
D^\mu q_L^f &= \left[\partial_\mu + i g_s \lambda_i A_i^\mu / 2 + i g \sigma_i W_i^\mu + \tfrac{1}{6} g' B^\mu\right] q_L^f \\
D^\mu u_R^f &= \left[\partial_\mu + i g_s \lambda_i A_i^\mu / 2 + \tfrac{2}{3} g' B^\mu\right] u_R^f \\
D^\mu d_R^f &= \left[\partial_\mu + i g_s \lambda_i A_i^\mu / 2 - \tfrac{1}{3} g' B^\mu\right] d_R^f
\end{aligned} \tag{2.109}$$

As with the standard electroweak theory, the quark mass is neglected in (2.107). In analogy with (2.103) the quark masses are introduced via Yukawa interactions:

$$\mathcal{L}^{qH} = -Y_f j^d \bar{q}^f \Phi d_R^j - -Y_f j^u \bar{q}^f \tilde{\Phi} u_R^j + h.c \tag{2.110}$$

Here, d_R^j and u_R^j are three component fields, including all three generations, and indexed by j ($u_R^j = (u_R, c_R, t_R)$).

The Standard Model is the combination of Lagrangian densities we have introduced in section. 2.1.3, 2.1.4 and 2.1.5:

$$\mathcal{L}^{SM} = \mathcal{L}^L + \mathcal{L}^q + \mathcal{L}^{LH} + \mathcal{L}^{qH} + \mathcal{L}^B + \mathcal{L}^G + \mathcal{L}^H ... \tag{2.111}$$

Of course, to obtain the complete Lagrangian density for the Standard Model, we need to add additional terms such as gauge fixing terms and ghosts term, which were not discussed here.

2.2 The Minimal Supersymmetric Standard Model (MSSM)

In this section, some problems of the Standard Model will be discussed. A solution to the problems is to introduce a supersymmetric Lagrangian, and promote the Standard Model to a supersymmetric theory. The details of the Minimal Supersymmetric Standard Model is given in (Murayama, 2000).

2.2.1 Problems of Standard Model

The Standard Model, although successful at predicting experimental observables, has been regarded as a low-energy effective theory of a fundamental theory. One thing which seems bizarre in the Standard Model is the assignment of the hypercharges. The hypercharges are quantized in units of 1/6, but in principle, can be any number. The quantized hypercharges are however, responsible for neutrality of bulk matter. The gauge group poses also questions. Why are there three independent gauge group, which conspire together to have anomaly-free particle content in a non-trivial way, and why is the strong interaction "strong" and weak interaction "weak"?

Another problem in the Standard Model arises when we look at the Higgs self-energy. The mass squared parameter μ^2 in (2.78) receives a quadratically divergent contribution from its self-energy corrections. Consider the process where the Higgs doublet splits into a pair of top quarks and recombine back to the Higgs boson. The self-energy correction is:

$$\Delta\mu_{top}^2 = -6\frac{h_t^2}{4\pi^2}\frac{1}{r_H^2} \tag{2.112}$$

where r_H is the "size" of the Higgs boson and h_t is the top quark Yukawa coupling. This makes the Standard Model not applicable below the distance scale of 10^{-17} cm. The motivation of supersymmetry is to make the Standard Model applicable to much shorter distances so that we may hope to find answers to puzzles in the Standard Model given by physics at short distance scales. In order to do so, we double the degrees of freedom with an explicitly broken symmetry. The top quark then receives a superpartner: stop. The loop diagram of the stop gives the contribution to the Higgs self-energy:

$$\Delta\mu_{stop}^2 = +6\frac{h_t^2}{4\pi^2}\frac{1}{r_H^2} \tag{2.113}$$

The linearly divergent piece $1/r_H$ cancels, and the total correction becomes:

$$\Delta\mu^2 = \Delta\mu_{top}^2 + \Delta\mu_{stop}^2 = -6\frac{h_t^2}{4\pi^2}(m_{\tilde{t}}^2 - m_t^2)log\frac{1}{r_H^2 m_{\tilde{t}}^2} \tag{2.114}$$

Now the correction only depends logarithmically on the "size" of the Higgs boson. The mass of the stop $m_{\tilde{t}}$ is not known. However, in order for $\Delta\mu^2$ to be in the same order as the tree value $\mu^2 = -2\lambda v^2$, we need $m_{\tilde{t}}^2$ to be not too far above the electroweak scale.

2.2.2 Supersymmetric Lagrangian

Supersymmetry is a symmetry between fermions and bosons, and relates particles with different spins. In supersymmetric theories, all particles fall into supermultiplets, which have both fermionic and bosonic components. Two types of supermultiplets appear in renormalizable theories: the chiral and vector supermultiplets.

Chiral supermultiplets are often denoted with ϕ and contain three fields: a complex scalar field A, a Weyl fermion $P_L\psi = \psi$, and an auxiliary complex field F. The Lagrangian for chiral supermultiplets consists of two parts, Kähler potential and a superpotential. The Kähler potential is the kinetic terms for the fields, usually written with the short hand notation $\int \phi_i^* \phi_i d^4\theta$

$$\mathcal{L} \supset \int \phi_i^* \phi_i d^4\theta = \partial_\mu A_i^* \partial^\mu A_i + \bar{\psi}_i i \not{\partial} \psi_i + F_i^* F_i \qquad (2.115)$$

The superpotential is defined by a holomorphic function $W(\phi)$ of the chiral supermultiplets ϕ_i.

$$\mathcal{L} \supset \int W(\phi) d^2\theta = -\frac{1}{2} \left. \frac{\partial^2 W}{\partial\phi_i \partial\phi_j} \right|_{\phi_i = A_i} \psi^i \psi^j + \left. \frac{\partial W}{\partial\phi_i} \right|_{\phi_i = A_i} F_i \qquad (2.116)$$

The first term describes the Yukawa coupling of the bosonic and fermionic components of the chiral supermultiplets. Using (2.115) and (2.116), and solve for F, we find:

$$F_i^* = - \left. \frac{\partial W}{\partial\phi_i} \right|_{\phi_i = A_i} \qquad (2.117)$$

We can substitute it back to the Lagrangian, eliminating F and we find

the potential term:

$$\mathcal{L} \supset -V_F = -\left|\frac{\partial W}{\partial \phi_i}\right|^2_{\phi_i = A_i} \tag{2.118}$$

The vector supermultiplet W_α is a generalization of the gauge fields, and consists of three components, a Weyl fermion (gaugino) λ, a vector gauge field A_μ, and an auxiliary real scalar field D. A short-hand notation for the kinetic term is:

$$\mathcal{L} \supset \int W_\alpha^a W^{\alpha a} = -\frac{1}{4}F_{\mu\nu}\bar{\lambda}^a i \slashed{D} \lambda^a + \frac{1}{2}D^a D^a \tag{2.119}$$

Since the vector supermultiplets contain gauge fields, chiral supermultiplets which transform non-trivially under gauge transformation, must couple with the vector supermultiplets in order for the Lagrangian to be gauge invariant. The Kähler potential potential must be modified from $\int \phi_i^* \phi_i d^4\theta$ to $\int \phi_i^\dagger e^{2gV} \phi_i d^4\theta$. Here, V is another short-hand notation of the vector multiplet. The Kähler potential in (2.115) is modified to:

$$\mathcal{L} \supset \int \phi_i^\dagger e^{2gV} \phi_i d^4\theta =$$
$$D_\mu A_i^\dagger D^\mu A_i + \bar{\psi}_i i \slashed{D} \psi_i + F_i^\dagger F_i - \sqrt{2}g(A^\dagger T^a \lambda^a \psi) - gA^\dagger T^a D^a A \tag{2.120}$$

We can use equation (2.119) and (2.120) to solve for D^a, substitute it back to the Lagrangian to eliminate it gives the potential term V_D:

$$\mathcal{L} \supset -V_D = -\frac{g^2}{2}(A^\dagger T^a A)^2 \tag{2.121}$$

The general supersymmetric Lagrangians are given by (2.118), (2.120) and (2.121).

2.2.3   The Minimal Supersymmetric Standard Model

Now, we promote the Standard Model to a supersymmetric model. The Minimal Supersymmetric Standard Model is a supersymmetric version of

the Standard Model with minimal particle content. The first task is to promote all fields in the Standard Model to the appropriate supermultiplets. For gauge bosons, they all become vector multiplets. In the Standard Model we have both left- and right-handed fields, thus in order to promote them to chiral supermultiplets, we need make all fields left-handed Weyl spinors. This is done by charge-conjugating all right-handed fields. The Higgs boson can be embedded into a chiral supermultiplet H_u. It can couple to up-type quarks and generate their masses. In order to generate masses for down-type quarks we usually use (2.104). This trick does not work in supersymmetry as the superpotential W must be a holomorphic function of the chiral supermultiplets and one cannot take a complex conjugation of this sort. We need to introduce another chiral supermultiplet H_d. The chiral supermultiplets in MSSM are summarized in Table 1.

$L_1(1,2)^{-1/2}$	$L_2(1,2)^{-1/2}$	$L_3(1,2)^{-1/2}$
$E_1(1,1)^{+1}$	$E_2(1,1)^{+1}$	$E_3(1,1)^{+1}$
$Q_1(3,2)^{1/6}$	$Q_2(3,2)^{1/6}$	$Q_3(3,2)^{1/6}$
$U_1(3,1)^{-2/3}$	$U_2(3,1)^{-2/3}$	$U_3(3,1)^{-2/3}$
$D_1(3,1)^{+1/3}$	$D_2(3,1)^{+1/3}$	$D_3(3,1)^{+1/3}$
	$H_u(1,2)^{+1/2}$	
	$H_d(1,2)^{-1/2}$	

Table 1: The Chiral Supermultiplets in the MSSM. The numbers in parenthesis refer to SU(3) and SU(2) representations. The superscript are supercharges

The superpotential allowed by the SU(3) $\times$ SU(2) $\times$ U(1) gauge invariance and after imposing R-parity is:

$$W = \lambda_u^{ij} Q_i U_j H_u + \lambda_d^{ij} Q_i D_j H_d + \lambda_e^{ij} L_i E_j H_d + \mu H_u H_d \qquad (2.122)$$

The first three terms are recognized as the Yukawa couplings in the Standard Model. The parameter μ has a mass dimension one and gives a supersymmetric mass to both bosonic and fermionic components of the H_d and H_u supermultiplets.

As we have not seen any superpartners of the Standard Model particles, we need to add soft-breaking terms to the Lagrangian. Assuming R-parity

they are given by:

$$\mathcal{L}_{soft} = \mathcal{L}_1 + \mathcal{L}_2$$
$$\mathcal{L}_1 = -m_Q^{2ij}\tilde{Q}_i^*\tilde{Q}_j - m_U^{2ij}\tilde{U}_i^*\tilde{U}_j - m_D^{2ij}\tilde{D}_i^*\tilde{D}_j - m_L^{2ij}\tilde{L}_i^*\tilde{L}_j - m_E^{2ij}\tilde{E}_i^*\tilde{E}_j - m_{H_u}^2|H_u|^2 - m_{H_d}^2|H_d|^2$$
$$\mathcal{L}_2 = -A_u^{ij}\lambda_u^{ij}\tilde{Q}_i\tilde{U}_jH_u - A_d^{ij}\lambda_d^{ij}\tilde{Q}_i\tilde{D}_jH_d - A_l^{ij}\lambda_e^{ij}\tilde{Q}_i\tilde{U}_jH_d + B\mu H_uH_d + c.c$$
$$(2.123)$$

The mass-squared parameters for scalar quarks and scalar leptons are 3×3 hermitian matrices. The trilinear couplings A^{ij} and bilinear coupling B are general complex numbers.

MSSM introduces a superpartner for each particle in the Standard Model. The quarks and leptons in SM are called in their usual way, while their superpartner adds a prefix "s" (which stands for scalar) to each of their fermionic counterpart. Their symbols are denoted the same as SM, but with added tilde. For example, the superpartner of an electron is a selectron, and it is written as $\tilde{e}$. The superpartner of the Higgs doublets are called higgsinos. In general, fermionic partners of bosons in the SM have "ino" at the end of their name. The superpartners to gauge bosons are called gauginos. The corresponding superpartner name for each gauge bosons are: gluino for gluon, wino for W and bino for B. Due to electroweak symmetry breaking, all neutral "inos" i.e, the two neutral higgsinos, the neutral wino $\tilde{W}^3$ and the bino $\tilde{B}$ mix with each other to form four Majorana fermions (i.e a fermion which is its own anti-particle). They are called neutralinos $\tilde{\chi}_i^0$, $i = 1, 2, 3, 4$. The charged higgsinos and the charged winos $\tilde{W}^-$, $\tilde{W}^+$ mix and form two massive Dirac fermions called charginos: $\tilde{\chi}_i^\pm$, $i = 1, 2$. A consequence of imposing R-parity is that the Lightest Supersymmmetric Particle (LSP) is stable. If we require the LSP to be electrically neutral and weakly interacting, then the LSP should be a superpartner to Z, γ or neutral Higgs bosons or their linear combination neutralino ($\tilde{\chi}_1^0$). The LSP is thus a good candidate for the Cold Dark Matter.

3   Experiment framework

3.1   The CERN Large Hadron Collider (LHC)

A detailed description of the LHC can be found in (Evans and Bryant, 2008). The Large Hadron Collider (LHC) is a two-ring superconducting hadron accelerator and collider. It is installed in the existing 26.7 km tunnel that was constructed between 1984 and 1989, which was originally built for LEP, and it also re-uses the injection chain from LEP. The LEP machine was discontinued in 2000 to liberate the tunnel for LHC. The LHC is designed to collide proton beams at a center-of-mass energy of up to 14 TeV at luminosity of $10^{34} cm^{-2} s^{-1}$ and heavy (Pb) ions with an energy of up to 2.8 TeV per nucleon.

The LHC design depends on basic principle linked to the latest technology. As it is a particle-particle collider, there are two rings with counter-rotating beams, in contrast to particle-antiparticle colliders which can have both beams sharing the same phase space in a single ring. The tunnel geometry was originally designed for electron-positron machine LEP, and there where eight crossing points flanked by long straight sections for RF cavities that compensated the high synchrotron radiation losses. A proton machine such as LHC would not have the same synchrotron radiation problem and would ideally, have longer arcs and shorter straight section for the same circumference. But, as a cost-effective solution, the tunnel was accepted as it was. It was decided to equip only four of the possible eight interaction regions and to suppress beam crossings in the other four to prevent disrupting the beams.

The number of events generated per second in LHC collisions is given by:

$$N_{events} = L\sigma_{event} \tag{3.1}$$

where σ_{event} is the cross-section for the relevant event and L is the machine luminosity given by:

$$L = \frac{N_b^2 n_b f_{rev} \gamma_r}{4\pi\epsilon_n \beta^*} F \tag{3.2}$$

where N_b is the number of particles per bunch, f_{rev} is the revolution frequency, n_b is number of bunches per beam, γ_r is the relativistic gamma factor, ϵ_n is the normalized transverse beam emittance, β^* is the beta function at the collision point, and F is the geometric luminosity reduction factor due to the crossing angle at the interaction point. There are two high luminosity experiments dedicated to proton-proton collisions: ATLAS and CMS. During Run 2 of the LHC in the years 2015-2018, the peak luminosity recorded was 5 to $19 \times 10^{33} cm^{-2} s^{-1}$ with maximum number of colliding bunches of 1544 in 2018 (The ATLAS collaboration, 2019). LHC has one experiment dedicated to ion collisions, ALICE, which aims at a peak luminosity of $L = 10^{27} cm^{-2} s^{-1}$.

The integrated luminosity is given by:

$$L_{int} = L_0 \tau_L \left[1 - e^{-T_{run}/\tau_L} \right] \tag{3.3}$$

where τ_L is the luminosity lifetime, L_0 is the luminosity at the start of the run and T_{run} is the total duration of the run.

3.2 ATLAS detector

The details of the ATLAS detector is described in (The ATLAS Collaboration, 2008). It is a multipurpose detector built for probing p-p and A-A collisions. The detector is forward-backward symmetric with respect to the interaction point and has a solid angle coverage of almost 4π.

The coordinate system used to describe the ATLAS detector and particles emerging from p-p collision defines the nominal interaction point as the origin of the system. The beam direction defines the z-axis and the x-y plane is transverse to the beam direction. The positive x-axis direction is defined as pointing from the interaction point to the center of the LHC-ring, while the positive y-axis is defined as pointing upwards. The azimuth angle ϕ is measured around the beam axis, and the polar angle θ is the angle from the beam axis. The pseudo rapidity is defined as $\eta \equiv -ln\left(tan\left(\frac{\theta}{2}\right)\right)$. The transverse momentum p_T and the transverse energy E_T are defined in the x-y-plane.

The inner detector (ID) is immersed in a $2T$ magnetic field generated by the central solenoid. Pattern recognition, momentum- and vertex mea-

surement, and electron identification are achieved through a combination of discrete, high-resolution semi-conductor pixel and strip detectors (SCT) in the inner-volume and straw-tube tracking (TRT) detectors it its outer part. The precision tracking detectors, pixel and SCT, cover a region of $|\eta| < 2.5$. The straw-tube tracking detector in the outer part of the inner detector is capable of generating and detecting transition radiation.

The inner detector is surrounded by a high granularity liquid-argon (LAr) electromagnetic sampling calorimeter. It covers the pseudorapidity range of $|\eta| < 3.2$. The EM calorimeter is divided into a barrel part with $|\eta| < 1.475$ and two end-cap components covering $1.375 < |\eta| < 3.2$. Hadronic calorimetry is provided by a scintillator-tile calorimeter, covering a range of $|\eta| < 1.7$, and it is placed directly outside the EM calorimeter envelop. The tile calorimeter is divided into a large barrel and two smaller extended barrel cylinders, one on either side of the central barrel. Located behind the end-cap EM calorimeter is the Hadronic End-cap Calorimeter (HEC). To reduce the drop in material density at the transition between the end-cap and forward calorimeter, the HEC extends out to $|\eta| = 3.2$. The HEC also overlaps with the tile calorimeter by extending to $|\eta| = 1.5$. The LAr forward calorimeter (FCal) provides both electromagnetic and hadronic energy measurements, and extends the pseudorapidity coverage to $|\eta| = 4.9$

Surrounding the calorimeter is the muon spectrometer. It is based on the magnetic deflection of muon tracks in the large superconducting air-core-toroid magnets, instrumented with separate trigger and high-precision tracking chambers. In the barrel region, tracks are measured in chambers arranged in three cylindrical layers around the beam axis. In the transition and end-cap regions, the chambers are installed in planes perpendicular to the beam in three layers. The overall dimension of the ATLAS detector is defined by the muon spectrometer.

The proton-proton interaction rate at design luminosity of $10^{34} cm^{-2} s^{-1}$ is approximately 1 GHz. Event data recording is limited to around 1 kHz due to limitation in technology and resources. In Run 2 a two-stage trigger system, the Level-1 (L1) and the High-Level trigger (HLT), is used to reduce the data-taking rate. The first stage is the L1 trigger which accepts events at a rate up to the maximum detector read-out rate of 100 kHz, reducing it from the bunch crossing rate of about 40 MHz. The L1 trigger uses information from a subset of detectors, and searches for high p_T muons, electrons, photons, jets, and τ-leptons decaying into hadrons, as well as large missing and total transverse energy. In addition to event selections, the L1 trigger defines one

or more Regions of-Interest (RoI's) in η and ϕ in each events. The ROI's are then passed on to the second stage of the trigger. The HLT trigger is software-based, and investigates the ROI's from the first trigger stage. All available data from the sub-detectors in the ROI's are used in the HLT trigger. The data recording rate is reduced to on average 1.2 kHz by the HLT trigger (The ATLAS collaboration, 2020).

4 Simulation

4.1 Simulated event samples

Simulated Monte Carlo (MC) event samples are used to model both SUSY signals and SM background samples. All MC samples were generated at $\sqrt{s} = 13$ TeV.

A simplified model of squark pair production is considered. In this model the squarks undergo a two-step decay leading to τ-leptons and LSP. A Feynman diagram of the simplified model is shown in Figure 1. The squarks are assumed to decay to $q\tilde{\chi}_1^{\pm}$ and $q\tilde{\chi}_2^0$ with same branching ratios. The neutralinos $\tilde{\chi}_2^0$ decays to $\tilde{\tau}\tau$ and $\tilde{\nu}_\tau\nu_\tau$ with equal branching ratios, and the charginos $\tilde{\chi}_1^{\pm}$ are assumed to decays to $\tilde{\nu}_\tau\tau$ and $\tilde{\tau}\nu_\tau$ with equal probability. Finally, the staus $\tilde{\tau}$ and τ-sneutrinos $\tilde{\nu}_\tau$ are assumed to decay to $\tilde{\chi}_1^0\tau$ and $\tilde{\chi}_1^0\nu_\tau$, respectively. In this analysis 4 light squark species are considered and the others are kinematically decoupled. In addition, only superpartners of left-handed quarks are considered. The two free parameters of the model is the mass of the LSP $m_{\tilde{\chi}_1^0}$ and the mass of the squark $m_{\tilde{q}}$. The masses of $\tilde{\chi}_1^{\pm}$, $\tilde{\chi}_2^0$, $\tilde{\tau}$ and $\tilde{\nu}_\tau$ are set to:

$$m_{\tilde{\chi}_1^{\pm}} = m_{\tilde{\chi}_2^0} = \tfrac{1}{2}\left(m_{\tilde{q}} + m_{\tilde{\chi}_1^0}\right), \quad m_{\tilde{\tau}} = m_{\tilde{\nu}_\tau} = \tfrac{1}{2}\left(m_{\tilde{\chi}_1^{\pm}} + m_{\tilde{\chi}_1^0}\right) \tag{4.1}$$

Three signal samples of different mass scenarios in the signal model were produced on the fly (OTF), i.e the matrix element (ME) calculations, parton shower (PS) and event generation are done in one step. These samples were produced in Athena release 19, and they were used for SR optimization (see Section 6). The three benchmark samples were reproduced along with rest of the points in the signal grid using LHE files as input, during which ATLAS was in a transition period between 2 software releases concerning event sample generation, release 19 and release 21. Thus, we had to migrate the technical setup for squark signal from the old release to the new release. To ensure that the samples produced in Athena release 21, with the new technical setup, are consistent with the samples produced in release 19, we have produced validation plots, which compares the kinematic distributions of both releases. Athena release 21 uses the NNPDF30NLO PDF set by default, as opposed to release 19 which uses the NNPDF23LO PDF set. Figure 2 compares the kinematic distribution of MET and m_T^τ for Athena release

34

21 and 19. Here, the release 21 sample uses the default PDF set, and the difference in choice of PDF sets causes inconsistency between the samples generated in release 21 and 19. Kinematic distributions where the release 21 sample uses the same PDF set (NNPDF23LO) as in release 19 are shown in Figure 3, and shows much greater compatibility between the samples.
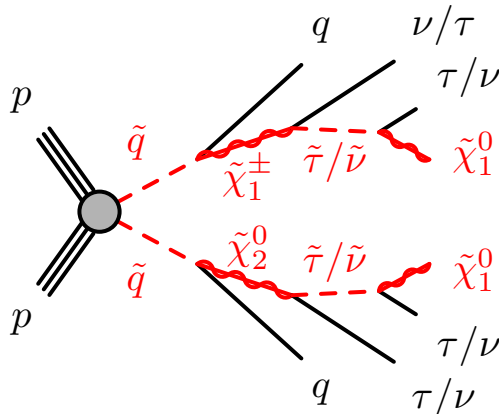

Figure 1: Feynman diagram illustrating the simplified model of decaying squark pair considered in this analysis.

In addition to migrating the setup from release 19 to 21, the setup was also modified to generate samples using common Les Houches Event (LHE) files as input. These files were generated beforehand using $MadGraph5\_aMC@NLO$ v2.6.2 and $Pythia$ 8.235 by the SUSY group. The LHE files includes all the matrix element (ME) calculations performed at tree level, which includes emission of one or two additional partons. Furthermore, all the production results (e.g parton-level information about hard processes) are stored in the LHE files. These LHE files can then be read and the squark decay, PS and event generation can be done skipping the ME calculation step in OTF generation, thus significantly reducing the computation time needed for squark signal sample generation. The squark decays and the masses of the sparticles in the decay chain are specified by the user. Compatibility between samples generated OTF and samples generated using LHE files has been investigated to validate the migration of the technical setup. Figure 4 show the MET and m_T^τ distribution for samples generated OTF and samples using LHE files as input, and shows great compatibility.

The event decays for the new signal samples (using LHE files) were done using $MadGraph5\_aMC@NLO$ v2.8.1 with $Pythia$ 8.244. The events were generated using the A14 tune for the modelling of hadronisation and

parton shower (PS), and the parton density function (PDF) set used is NNPDF23LO. ME-PS matching were done using the CKKW-L algorithm, with a matching scale set to one-fourth of the squark mass. The nominal cross-sections and the uncertainty were computed at NLO + NLL.
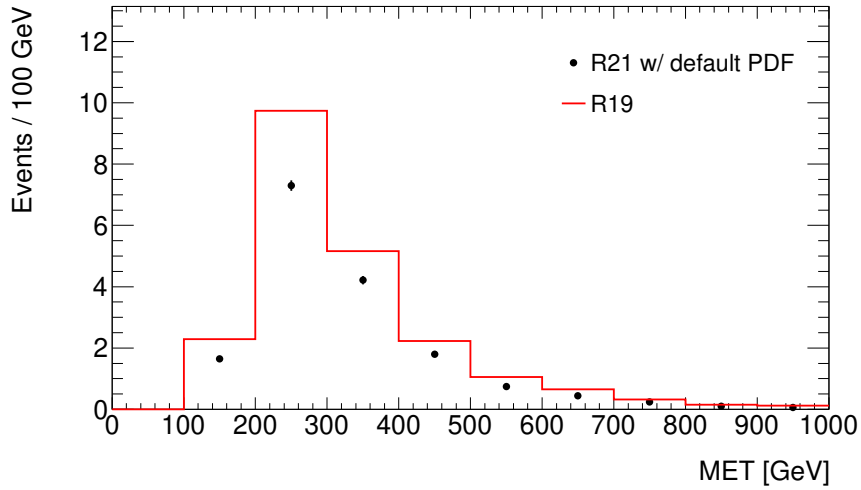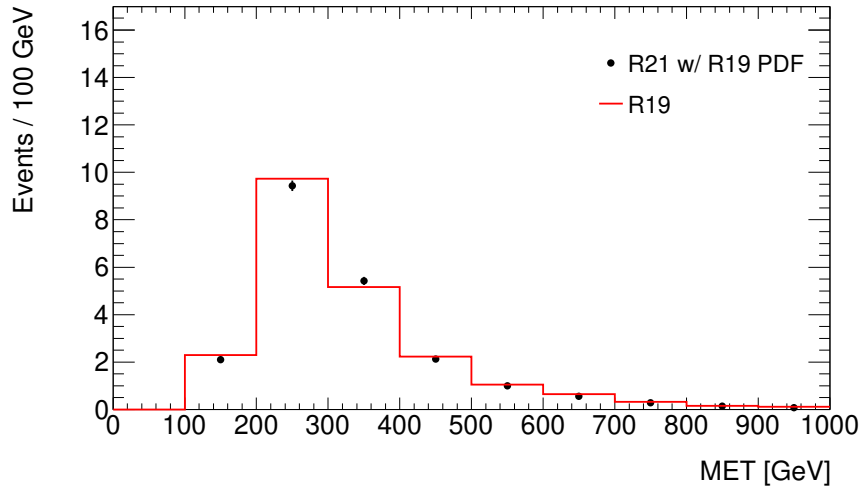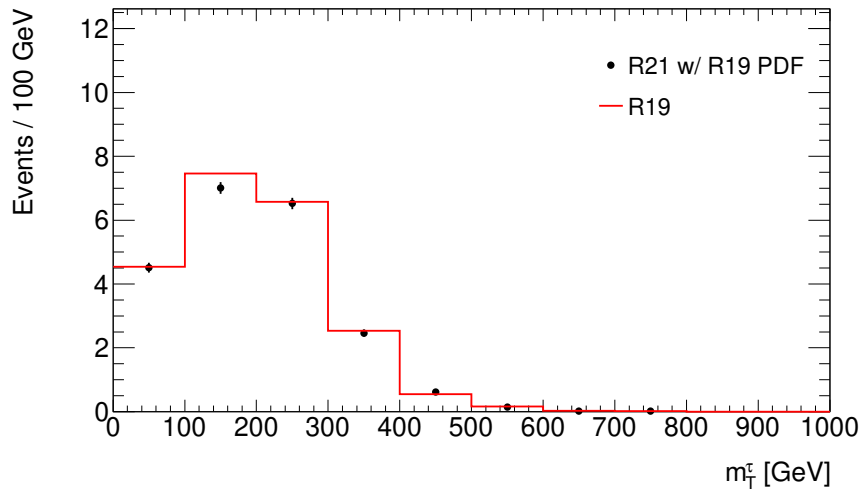

(a)
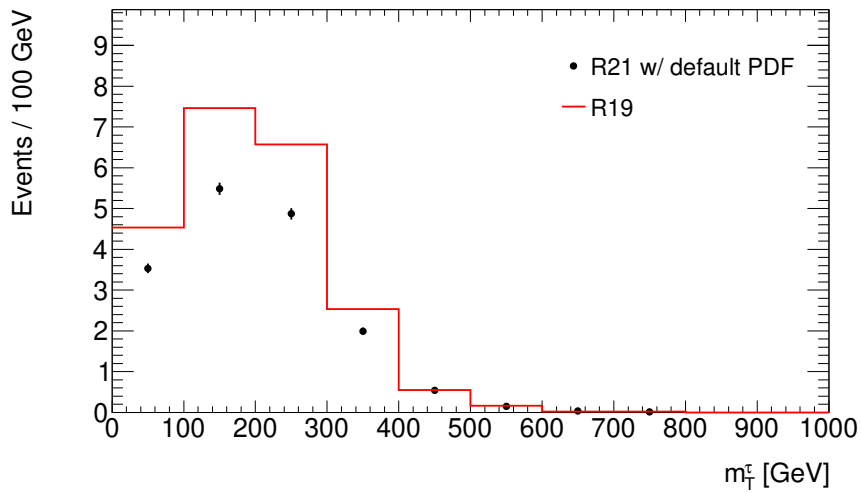
(b)

Figure 2: Kinematic distribution of MET (a) and m_T^τ (b) for Athena release 21 and 19. Here, the release 21 sample uses the NNPDF30NLO PDF set.
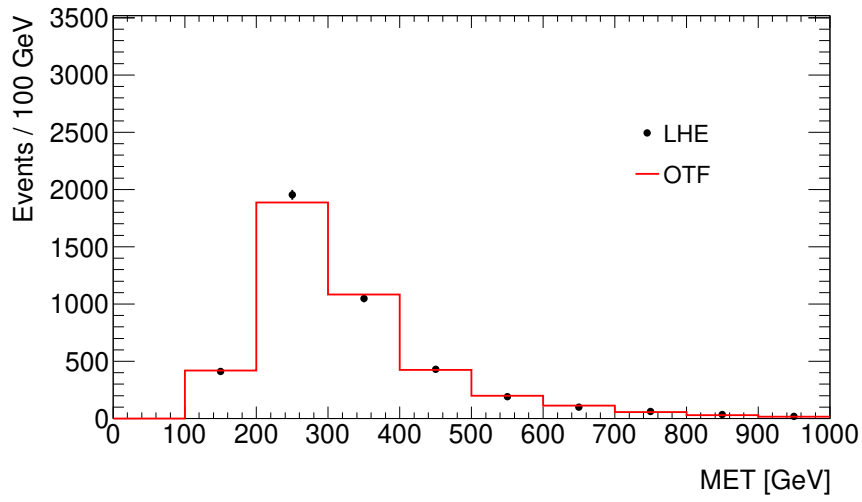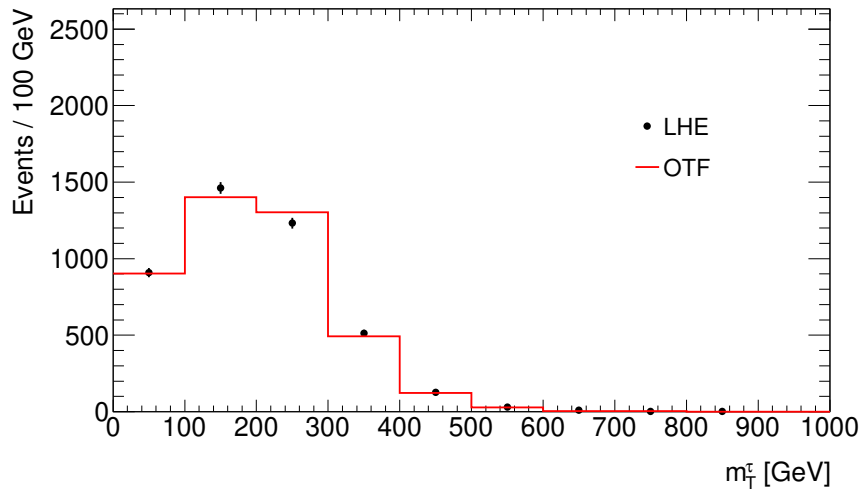
36

(a)

(b)

Figure 3: Kinematic distribution of MET (a) and m_T^τ (b) for Athena release 21 and 19. Here, the release 21 sample uses the NNPDF23LO PDF set.

37

(a)

(b)

Figure 4: Kinematic distribution of MET (a) and m_T^τ (b) for samples generated OTF and using LHE files as input.

4.2 Event reconstruction

This analysis is based on final states with jets, hadronically decaying τ-leptons, and missing transverse momentum (MET). Primary vertices are reconstructed using inner-detector tracks with transverse momentum $p_T > 500$ MeV. Primary vertex candidates are required to have at least two associated tracks, and the candidate with largest $\sum p_T^2$ is defined as the primary vertex. Events without a reconstructed primary vertex are vetoed.

The jets are reconstructed using the anti-k_t clustering algorithm using a distance parameter of $R = 0.4$. Jets are required to have $p_T > 20$ GeV and $|\eta| < 2.8$. To discriminate between hard-interaction jets from pileup jets, a jet-vertex-tagging algorithm is used.

Hadronically decaying τ-leptons are reconstructed from anti-k_t jets within $|\eta| < 2.5$ and are calibrated using the local cluster weighting technique. The τ-leptons candidates are reconstructed from clusters of calorimeter cells within a cone of $\Delta R \equiv \sqrt{(\Delta\eta)^2 + (\Delta\phi)^2} = 0.2$ centered on the jet axis. The τ-leptons are required to have $p_T > 20$ GeV, and candidates reconstructed within the transition region between the endcap and the barrel calorimeter $(1.37 < |\eta| < 1.52)$ are vetoed. This analysis uses loose ID requirement for the τ-leptons, which are later tighten to the medium ID requirement after the overlap removal.

Muon candidates are reconstructed in the region $|\eta| < 2.5$ and are required to have $p_T > 10$ GeV. The candidates are also required to pass a medium ID requirement.

Electron candidates are reconstructed from isolated energy deposits in the electromagnetic calorimeter, matched to an inner-detector track. The canditates are required to have $p_T > 10$ GeV and $|\eta| < 2.47$. Electrons reconstructed within the transition region between the endcap and the barrel calorimeters $(1.37 < |\eta| < 1.52)$ are discarded. The electrons are also required to pass a loose ID requirement.

The missing transverse momentum $\vec{p}_T^{miss}$, which its magnitude is denoted by E_T^{miss}, is defined as the negative vector sum of the transverse momentum of all identified physics objects (i.e electrons, muons, jets, τ-leptons) and an additional soft-term. The soft term is constructed from all the tracks with $p_T > 500$ MeV where the primary vertex is not associated with any known physics objects.

After reconstruction, an overlap removal procedure is applied to remove ambiguity in the case of the same object gets reconstructed with several different algorithms. The overlap of reconstructed objects is based on the distance $\Delta R \equiv \sqrt{(\Delta\eta)^2 + (\Delta\phi)^2}$ between the objects. First, τ-leptons are discarded if they overlap with electrons or muons with distance $\Delta R < 0.2$. If an electron and a muon share the same inner-detector track, the electron is discarded. Next, if an electron or a muon overlap with a jet with distance $\Delta R < 0.2$, the jet is discarded. Electron and muons in the vicinity ($\Delta R < 0.4$) of a jet are considered to be originated from secondary decays within the jet and are discarded. Finally, in the case of overlapping τ-leptons and jets , τ-leptons are kept. An overview of the successive steps in the overlap removal procedure is summarized in Table 2

Object discarded	Object kept	Matching condition
τ-lepton	electron	$\Delta R < 0.2$
τ-lepton	muon	$\Delta R < 0.2$
electron	muon	shares same inne-detector track
jet	electron	$\Delta R < 0.2$
electron	jet	$\Delta R < 0.4$
jet	muon	$\Delta R < 0.2$
muon	jet	$\Delta R < 0.4$
jet	τ-lepton	$\Delta R < 0.2$

Table 2: Summary of successive steps in the overlap procedure.

5 Approximated discovery significance using the Asimov data set

In order to determine whether a signal exists or not, one want design a signal region. In other words, a region of high discovery sensitivity. One quantifies this sensitivity by calculating the p-value or more commonly in particle physics, the equivalent significance Z. The formula for this significance is based on a test statistic using the profile likelihood ratio, and the expression is usually approximated using the Asimov dataset. The following description of the likelihood statistical test is taken from (Cowan et al., 2011).

In search for new physical processes, one measures the number of events assumed to follow a Poisson distribution with mean value $s + b$, where s is the number of signal events and b is the number of background events. One define the null hypothesis to be background only, i.e., $s = 0$ and test it against the alternative, which includes both the signal and the background $s + b$. The p-value is related to the discovery significance Z by:

$$Z = \Phi^{-1}(1 - p) \tag{5.1}$$

where Φ is the cumulative distribution of the standard Gaussian. One rejects the null hypothesis if the significance is above a certain threshold. To calculate the p-value, we use the test statistic q_0:

$$q_0 = \begin{cases} -2ln\lambda(0), & \hat{s} > 0 \\ 0 & \hat{s} < 0 \end{cases} \tag{5.2}$$

Here $\hat{s}$ is the maximum-likelihood estimator for a likelihood function L in the profile likelihood ratio $\lambda(s)$, with nuisance parameter θ:

$$\lambda(s) = \frac{L(s, \hat{\hat{\theta}})}{L(\hat{s}, \hat{\theta})} \tag{5.3}$$

Where θ is a maximum-likelihood estimator, and $\hat{\hat{\theta}}$ here denotes the value of θ which maximizes L for a specific s. The test statistic q_0 is defined in such a way so that it becomes larger for greater disagreement between data and

the hypothetical value of $s = 0$. This can be seen from the definition of $\lambda(s)$ in Eq.(5.3) where $\lambda(s)$ always lies between 0 for bad agreement and 1 for good agreement. The logarithm of λ is thus always negative, and from Eg.(5.2), the test statistic q_0 is postive and increases with increasing disagreement. The p-value can be calculated using the test statistic:

$$p = \int_{q_{0,obs}}^{\infty} f(q_0|0)dq_0 \tag{5.4}$$

Where $f(q_0|0)$ is the probability distribution function of the test statistic q_0 under the assumption of background-only hypothesis and $q_{0,obs}$ is the observed value of q_0 from data. Using Wald's approximation, one can show that the significance Z is approximately:

$$Z = \sqrt{q_0} \tag{5.5}$$

Valid in the large sample limit.

We can now calculate the significance by constructing a likelihood function which describes our measurements and use Eq.(5.2)(5.3)(5.5). The following derivation of the Asimov approximated significance is taken from (Cowan, 2012).

In our case, the background is not known and will be treated as a nuisance parameter. Since the background is not known, it can be adjusted to accommodate any observed events. This makes it impossible to reject the null hypothesis and must be constrained. To constraint the background, we measure the number of events m in the so-called control region where there is purely background and no signal. The measurement m can be related to the primary measurement $n = s + b$ if m follows a Poisson distribution with mean value τb, where τ is called a scale factor. The likelihood function is the product of the Poisson distribution of n and m.

$$L(s,b) = \frac{(s+n)^n}{n!}e^{-(s+b)}\frac{(\tau b)^m}{m!}e^{-(\tau b)} \tag{5.6}$$

The estimators for s and b, and the conditional estimator $\hat{\hat{b}}(0)$ can be

calculated from (5.6).

$$\hat{s} = n - \frac{m}{\tau}$$
$$\hat{b} = \frac{m}{\tau}$$
$$\hat{\hat{b}}(0) = \frac{n+m}{1+\tau}$$

(5.7)

Using Eq.(5.6) and (5.7) we can calculate the profile likelihood ratio Eg.(5.3), and from there, calculate q_0 (5.2). From (5.5) Using Eq(5.5), we get the following expression for the significance:

$$Z = \left[-2 \left(n \ln \left[\frac{n+m}{(1+\tau)n} \right] m \ln \left[\frac{\tau(n+m)}{(1+\tau)m} \right] \right) \right]^{\frac{1}{2}}$$

(5.8)

We now use the Asimov dataset, where the measurement n and m are equal to their expectation values $s + b$ and τb. We now get the Asimov approximated significance Z_A:

$$Z_A = \left[-2 \left((s+b) \ln \left[\frac{s+(1+\tau)b}{(1+\tau)(s+b)} \right] \tau b \ln \left[1 + \frac{s}{(1+\tau)b} \right] \right) \right]^{\frac{1}{2}}$$

(5.9)

The scale factor τ is related to the variance of b.

$$\tau = \frac{b}{\sigma_b^2}$$

(5.10)

plugging Eq.(5.9) into Eq.(5.8) to eliminate τ gives:

$$Z_A = \left[2 \left((s+b) \ln \left[\frac{(s+b)(b+\sigma_b^2)}{b^2 + (s+b)\sigma_b^2} \right] - \frac{b^2}{\sigma_b^2} \ln \left[1 + \frac{\sigma_b^2 s}{b(b+\sigma_b^2)} \right] \right) \right]^{\frac{1}{2}}$$

(5.11)

6 Signal selection and optimization

5 different signal regions (SRs) have been designed using a cut-based approach, where we enforce strict kinematic requirements in order to discriminate signal from background. To optimize this approach, we use the Asimov approximated significance (Eq. 5.11) as reference and try to maximize it. The SRs have been designed for two τ channels. The 1τ-channel which requires exactly 1 medium ID τ-lepton, and the 2τ-channel which requires 2 or more medium ID τ-leptons.

Preselection	
Trigger	$E_T^{miss} > 180$ GeV, $p_T^{jet_1} > 120$ GeV
Jets	$N_{jet} \geq 2$, $p_T^{jet_2} > 25$ GeV
Multijet events	$\Delta\phi(p_T^{jet_{1,2}}, p_T^{miss}) > 0.4$

Table 3: Summary of the pre-selection requirement applied to all SRs.

A preselection common to all SRs has been applied. Included in the preselection is a trigger plateau requirement where the events are required to pass a lowest-threshold missing transverse momentum trigger. The trigger is found to have an efficiency of greater than 99% when requiring $E_T^{miss} > 180$ GeV and a leading jet with $p_T > 120$ GeV. To ensure we only have well-constructed events in our regions an additional jet is required with $p_T > 25$ GeV. Furthermore, the two leading jets are required to be separated from p_T^{miss} by 0.4 in ϕ to suppress multijet background where the energy of one of the jet is mismeasured, which causes E_T^{miss} to point to the mismeasured jet in ϕ. The preselection requirements is summarized in Table 3.

Figure 5 shows kinematic distributions at pre-selection level for both τ channels. In the 1τ-channel, the dominant backgrounds are $W(\tau\nu)$ and $t\bar{t}$ production, with sub-dominant contribution from $Z \to \tau\tau$, $t\bar{t} + X$ and diboson production. The 2τ channel features dominant contribution from $t\bar{t}$, $Z \to \tau\tau$, $t\bar{t} + X$ and diboson productions and sub-dominant contribution from $W(\tau\nu)$ and single-top production.

Three signal models representing different regions of the SUSY parameter space have been chosen as benchmark scenarios for SR optimization. These are scenarios where the mass splitting between the squarks and the LSP are greater than 1000 Gev, around 400 GeV and less than 50 GeV. The associated SRs are called High-Mass SR (HMSR), Medium-Mass SR (MMSR) and Low-Mass SR (LMSR) respectively. The SRs are optimized by scanning
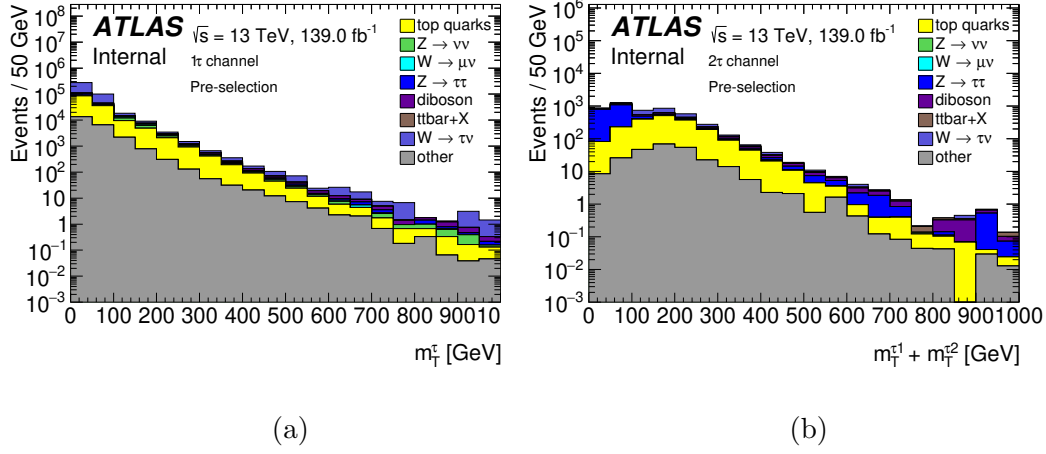
(a)   (b)

Figure 5: show kinematic distributions at pre-selection level. (a) shows the distribution of m_T^τ in the 1τ channel, and (b) shows the distribution of $m_T^{\tau_1} + m_T^{\tau_2}$ in the 2τ channel. The contributions labelled as other includes $Z \to ee$, $Z \to \mu\mu$, $W \to e\nu$ and single-top.

through different kinematic variables, and cut where the significance seems to be greatest. The significance was calculated according to Eq. 5.11, and based on uncertainty in the background yield according to previous similar SUSY analysis, assumes 40% uncertainty on the background. The kinematic variables used are defined in the following:

- The magnitude of the missing transverse momentum,

$$E_T^{miss}$$

- The transverse momentum of τ-leptons,

$$p_T^\tau$$

  in the 2τ channel the transverse momentum of the two highest τ-leptons are used.

- The transverse momentum of jets,

$$p_T^{jet}$$

- The total number of jets,

$$N_{jet}$$

45

- The transverse mass of the system formed by p_T^{miss} and the momentum of a lepton,

$$m_T^l \equiv m_T(\vec{p}_l, \vec{p}_T^{miss}) = \sqrt{2p_T^l E_T^{miss}(1 - cos\Delta\phi(\vec{p}_l, \vec{p}_T^{miss}))}$$

in the 1τ channel m_T^τ is used. The 2τ channel uses $m_T^{\tau_1} + m_T^{\tau_2}$ which is based on the two leading τ-leptons.

A cut on the transverse mass m_T^τ is applied to all SRs in the 1τ-channel. This requirement suppresses the dominant contribution of $W(\tau\nu)$ and $t\bar{t}$ production. A requirement on the magnitude of the missing transverse momentum (E_T^{miss}) is also applied to the 1τ-channel. The LMSR has a low $p_T^{\tau_1}$ requirement which exploits topologies where jets with high transverse momentum from initial-state radiation (ISR) recoils against the squark pair. In this situation, the τ-leptons and jets from squark decays may have low transverse momentum, but the LSP emitted may provides a substantial missing transverse momentum. Unique to HMSR, a requirement on $p_T^{jet_2}$ is also applied, while MMSR has an additional requirement on $p_T^{jet_3}$. The SR definition in the 1τ-channel is summarised in Table 4. The 2τ-channel SRs have requirements on $m_T^{\tau_1} + m_T^{\tau_2}$ which suppresses the dominant contributions from $t\bar{t}$, $Z \to \tau\tau$, $t\bar{t} + X$ and diboson production. A E_T^{miss} requirement is applied as well. The HMSR in this channel includes a $p_T^{jet_2}$ requirement, and the MMSR includes requirements on the p_T of both leading τ-leptons and on the total number of jets. No LMSR has been defined in this channel, as the expected sensitivity were too low. Table 5 summarises the SR requirements in the 2τ channel.

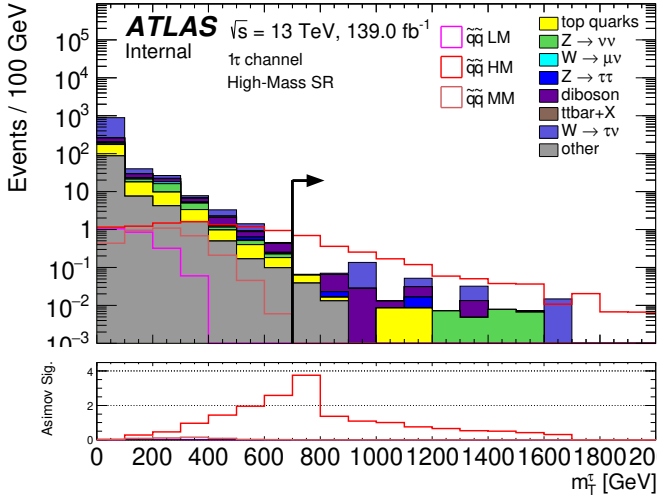|	1τ channel		
	$N_\tau^{medium} = 1$		
	High-Mass SR	Medium-Mass SR	Compressed SR
N_{jet}	-	≥ 4	-
$m_T^{\tau_1}$	> 700 GeV	> 250 GeV	> 100 Gev
E_T^{miss}	> 550 GeV	> 750 GeV	> 650 GeV
$p_T^{jet_2}$	> 250 GeV	-	-
$p_T^{jet_3}$	-	> 100 GeV	-
$p_T^{\tau_1}$	-	-	< 30 GeV

Table 4: Summary of requirements applied to SRs in the 1τ channel.

The distribution of m_T^τ for the three benchmark scenarios with the 1τ-channel SRs requirements applied, except for the m_T^τ requirement, is shown
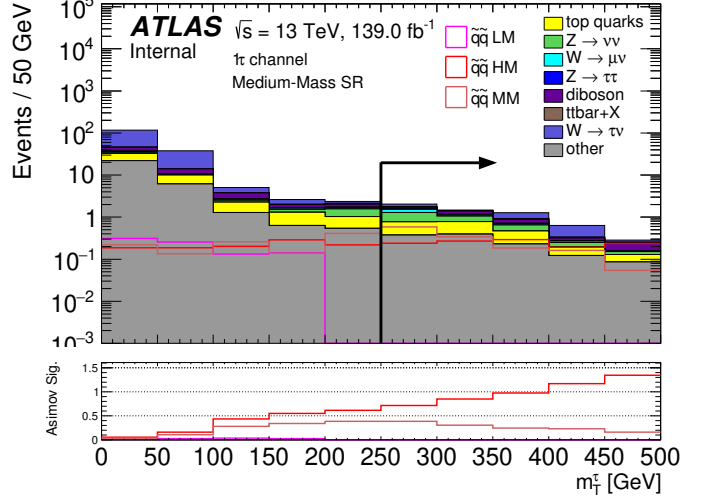
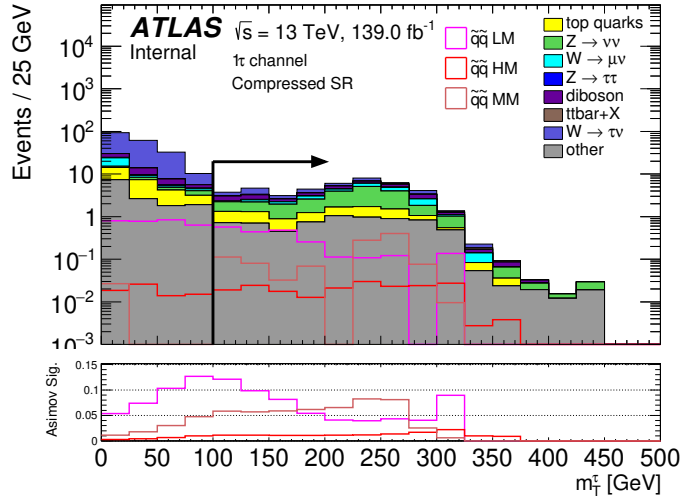| 2τ channel		
$N_\tau^{medium} \geq 2$		
	High-Mass SR	Medium-Mass SR
$m_T^{\tau_1} + m_T^{\tau_2}$	> 700 GeV	> 480 GeV
$p_T^{jet_2}$	> 300 GeV	-
$p_T^{\tau_1}$	-	< 100 GeV
$p_T^{\tau_2}$	-	> 35 GeV

Table 5: Summary of requirements applied to SRs in the 2τ-channel.

in figure 6. The plot at the bottom of the distributions shows the Asimov approximated significance from Eq. 5.11 if we cut at that specific value. The arrow shows the relevant selection cut for the different SRs, and the expected significance for the HM scenario in the HMSR is 3.75. In the MMSR the expected significance for the MM scenario is 0.38, while in the LMSR the expected significance is 0.12 for the LM scenario. Figure 7 shows the distribution of $m_T^{\tau_1} + m_T^{\tau_2}$ in the 2τ-channel and with SRs requirements applied, except for the $m_T^{\tau_1} + m_T^{\tau_2}$ requirement. As in figure 6, the bottom plot shows the Asimov approximated significance, and the expected significance in the HMSR for the HM scenario is 3.30. In MMSR the expected significance is 1.75 for the MM scenario.

(a)

(b)

(c)

Figure 6: Shows m_T^τ distributions for the three different benchmark scenarios. The distributions are shown with HMSR (a), MMSR (b), and LMSR (c) requirements applied except for the m_T^τ requirement in the 1τ-channel. The arrow shows the m_T^τ requirements for the SRs. The bottom figures show the Asimov approximated significance from Eq. 5.11 if we cut at the value.
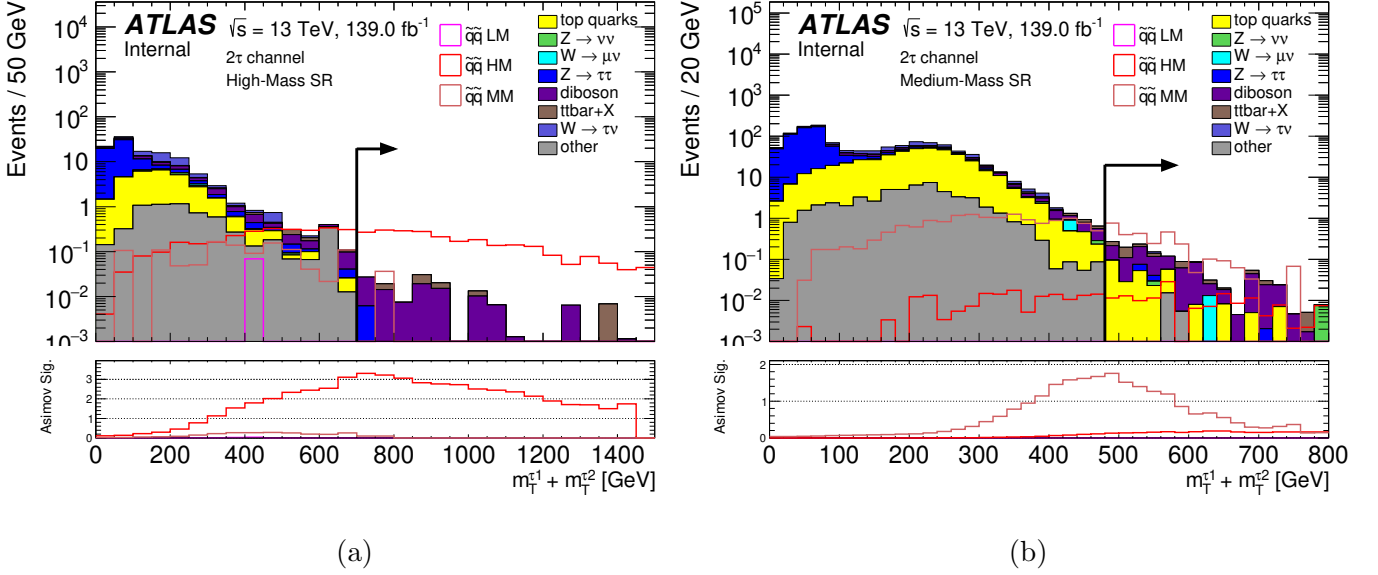
Figure 7: Shows $m_T^{\tau_1} + m_T^{\tau_2}$ distributions for the three different benchmark scenarios. The distributions are shown with HMSR (a)and MMSR (b) requirements applied except for the $m_T^{\tau_1} + m_T^{\tau_2}$ requirement in the 2τ-channel. The arrow shows the $m_T^{\tau_1} + m_T^{\tau_2}$ requirements for the SR. The bottom figures show the Asimov approximated significance from Eq. 5.11 if we cut at the value.

The SRs have been applied across the $(m_{\tilde{q}}, m_{\tilde{\chi}_1^0})$ parameter space. Figure 10 show the expected significance for different mass scenarios in the signal model when we apply the SR selection in the 1τ-channel. The best significance for large mass splitting is achieved when we apply the HMSR selections, while the significance in regions where the mass splitting is around 200 GeV, is largest for MMSR selections. The significance in the compressed points (near the diagonal) is largest for LMSR selections. Figure 9 shows the significance for different mass scenarios when we apply the 2τ-channel SRs. Again, the HMSR selection provides the best significance for high mass splitting, and the highest significance for intermediate mass splitting is achieved with MMSR selections. As expected, the SRs do well in the respective region they were designed for. However, the LMSR selection did not provide a substantial sensitivity for the compressed points, and re-optimization is desired. Figure 8 shows the best significance achieved by the SRs from Section 6 for different points in the parameter space. Based on the expected significance from Figure 8, we can expect to exclude signals up to squark mass at around 1600 GeV for low LSP mass.
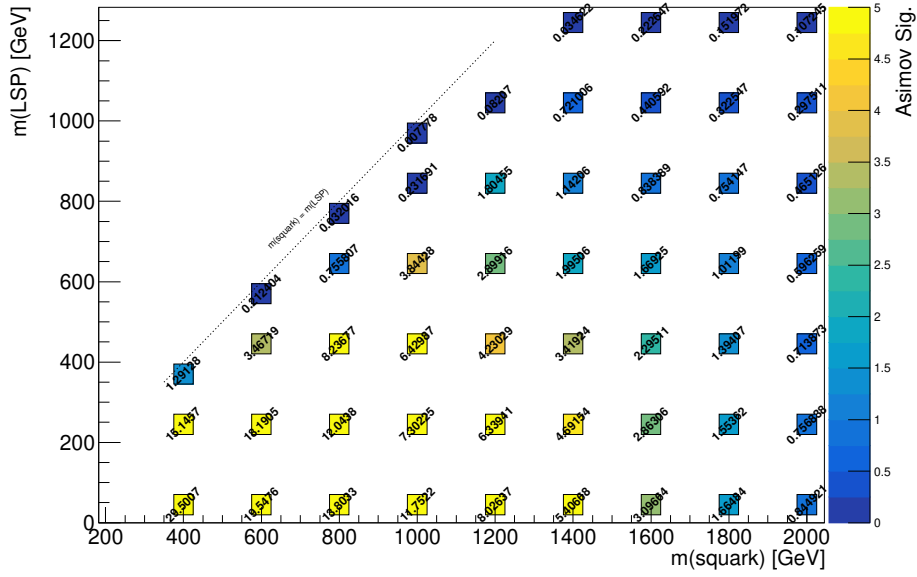
Figure 8: A 2D histogram of the best expected significance across the mass parameter space when the SRs are applied. The dashed line indicates where the squark mass is equal to the neutralino mass.

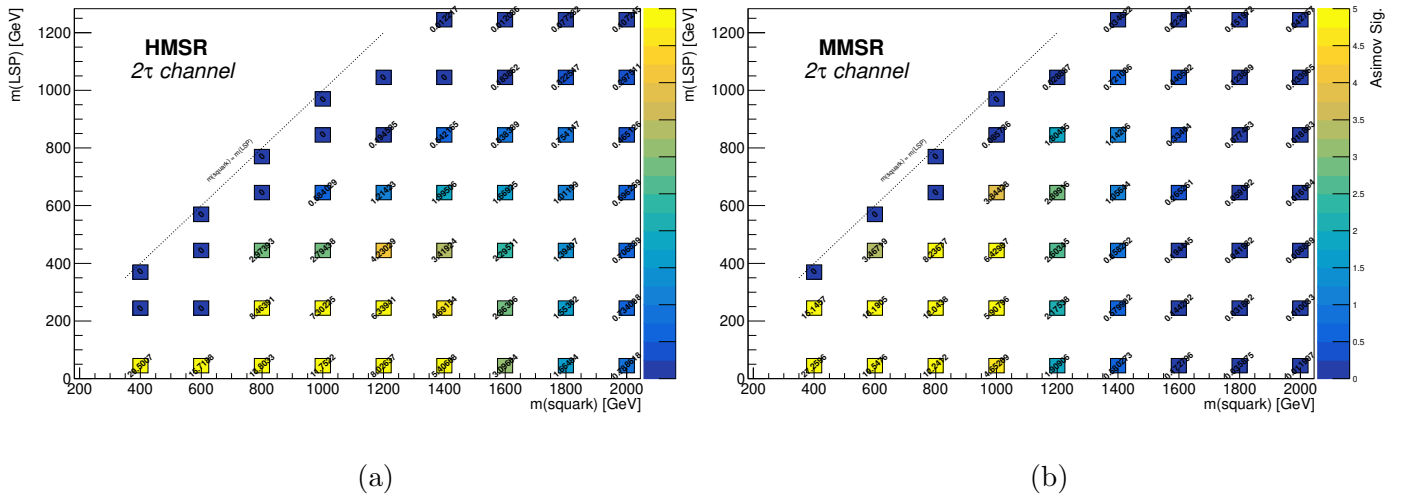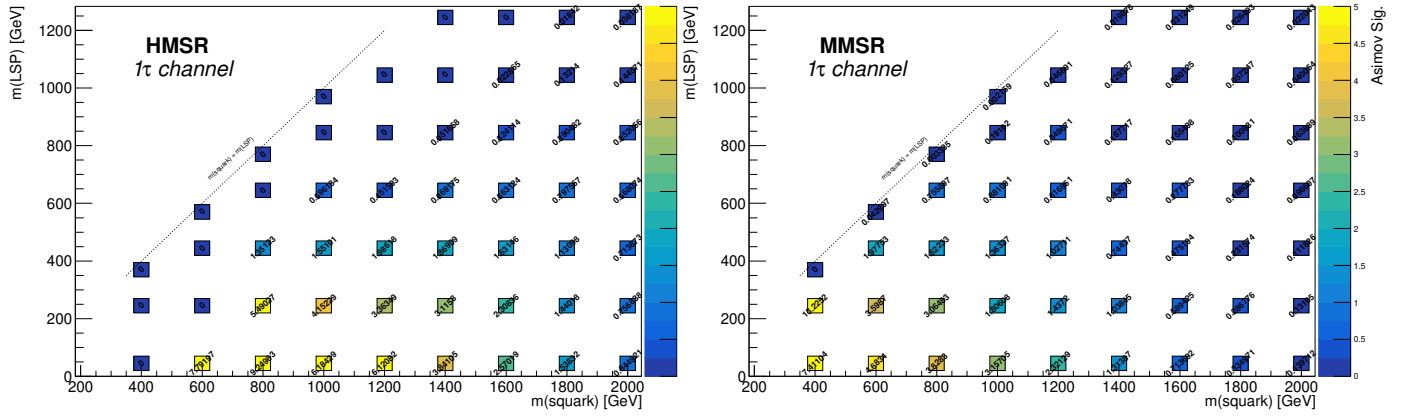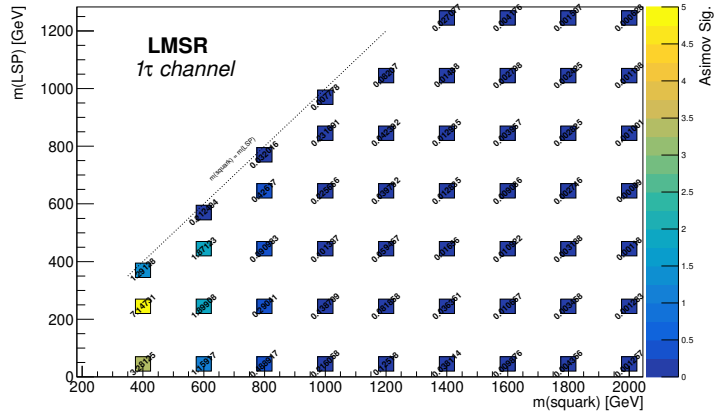(a)   (b)

Figure 9: Shows the Asimov approximated significance across different points in the $(m_{\tilde{q}}, m_{\tilde{\chi}_1^0})$ parameter for HMSR (a) and MMSR (b) in the 2τ-channel. The dashed line indicates where the squark mass is equal to the neutralino mass.

(a)

(b)

(c)

Figure 10: Shows the Asimov approximated significance across different points in the $(m_{\tilde{q}}, m_{\tilde{\chi}_1^0})$ parameter for HMSR (a), MMSR (b) and LMSR (c) in the 1τ-channel. The dashed line indicates where the squark mass is equal to the neutralino mass.

7 Results

An exclusion contour plot has been produced using only the SRs defined in Section 6. The exclusion contour is produced using the HistFitter framework (Baak et al., 2015). The profile likelihood ratio is used as a test statistic, and the CL_s method (Read, 2002) is used to derive the p-values. The systematic uncertainties are included using a Gaussian probability density function in the likelihood function and is treated as nuisance parameters. The likelihood function is given by:

$$L = P_{SR} \times P_{CR} \times C_{syst} \tag{7.1}$$

where P_{SR} and P_{CR} are the Poisson measurements in the signal region and control region respectively, and their expectation value depends on the nuisance parameters that parametrizes systematic uncertainties. P_{CR} is neglected as we only have SRs. The third term C_{syst} is the aforementioned Gaussian probability density functions.

Figure 11 shows an exclusion contour at 95% confidence level (CL), and is produced using only the SRs defined in Section 6, and the CL_s values were calculated for each parameter values and SRs separately. The best CL_s values achieved from the SRs were then interpolated between each point in the parameter space using a linear algorithm to produce the contour plot. Here, only experimental systematic uncertainties are considered, and the yellow band shows the standard-deviation spread around the median limit. The experimental systematic uncertainties includes uncertainties related to identification, reconstruction, calibration and corrections applied to jets, τ-leptons, muons, electrons and missing transverse momentum. The preliminary expected limit shows squark masses of up to around 1700 GeV are expected to be excluded for low LSP masses. LSP mass of up to about 800 GeV are expected to be excluded for squark masses around 1250 GeV. Figure 11 is consistent with the expected significance calculated across the parameter space from Figure 8. The expected significance drops below ~ 3 when moving to higher squark masses than 1600 GeV in the parameter space at LSP mass of 45 GeV. The significance drops below ~ 2.9 for LSP masses larger than 800 GeV at squark mass of 1200 GeV.
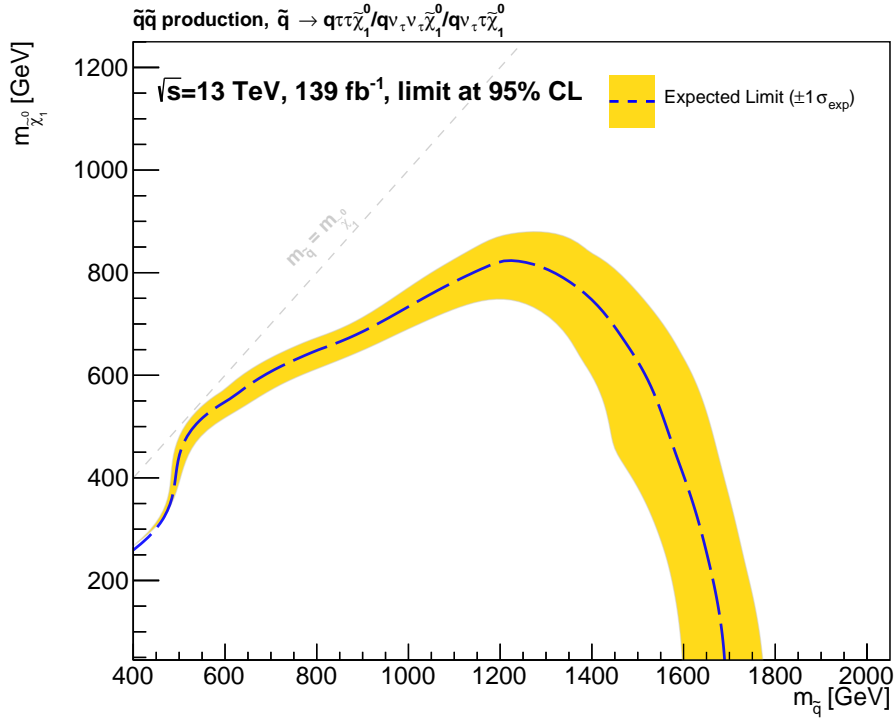
Figure 11: Exclusion contour showing expected exclusion limit at 95% CL using only SRs defined in Section 6. The yellow band shows the standard-deviation spread around the median limit. The limit is calculated using experimental systematic uncertainties.

8 Summary and Outlook

SRs have been designed and optimized using the Asimov approximated significance for search of squarks produced via strong interaction in events with jets, at least one hadronically decaying τ-lepton, and missing transverse momentum. The search is based on the full ATLAS Run 2 dataset of proton-proton collision at $\sqrt{s} = 13$ TeV with an integrated luminosity of 139 fb^-1. The SRs have been designed for two distinct topologies, the 1τ-channel and the 2τ-channel. The 1τ-channel requires only one τ-lepton in the final state, while the 2τ-channel requires two or more τ-leptons in the final state. Three points in the mass parameters space have been chosen for SR optimization. The three points are when the mass splitting between the squark mass and the LSP mass is greater than 1000 GeV (HMSR), around 400 GeV (MMSR) and less than 50 GeV (LMSR). No LMSR have been designed for the 2τ-channel as the expected significance were too low.

The signals were produced during transition between to software releases, release 19 and release 21. The technical setup for squark signal samples has been migrated from release 19 to 21. Validation plots showing kinematic distribution have been produced to compare the samples generated in the different releases. Release 21 uses a different PDF set (NNPDF30NLO) as opposed to release 19 which uses the NNPDF23LO PDF set, and the difference in PDF set causes inconsistency between the samples generated in release 19 and 21. Using the NNPDF23LO PDF set in release 21 showed much greater compatibility between release 21 and 19 samples. The new samples were also generated using LHE files, which reduces computation time significantly for signal generation compared to samples generated OTF. Compatibility between samples generated using LHE files as input files and samples generated OTF has been investigated, and kinematic distributions between the samples showed great compatibility.

The SRs were used to produce an exclusion contour plot at 95% confidence level. The preliminary result from SR-only exclusion plot shows that squark masses up to 1700 GeV are expected to be excluded for low LSP masses, and LSP masses up to 800 GeV are expected to be excluded when the squark mass is ~ 1300 GeV.

For a full analysis, the work remains to design control regions (CRs) for each of the dominant backgrounds for the background estimation and validation regions (VRs) to validate the background estimation. VRs are

regions "between" the SR and CR, where the background dominates, but with small signal contributions. The background is estimated through a normalization to data in a fit of CRs. The result of the fit can be extrapolated to the SRs or VRs using the so-called transfer factor. After good agreement in VR, the SRs can be unblinded to look for excess of data, which of course one wish to see in order to establish discovery or observation of the new physics. If there are no excess, we can redo the exclusion contour plot with SRs and CRs, and calculate the model-independent upper limit on the event yield for each SR.

References

M. Aaboud et al. Search for squarks and gluinos in final states with hadronically decaying τ-leptons, jets, and missing transverse momentum using pp collisions at $\sqrt{s} = 13$ TeV with the atlas detector. *Phys. Rev. D*, 99:012009, Jan 2019. doi: 10.1103/PhysRevD.99.012009. URL `https://link.aps.org/doi/10.1103/PhysRevD.99.012009`.

M. Baak, G. J. Besjes, D. Côté, A. Koutsman, J. Lorenz, and D. Short. Histfitter software framework for statistical data analysis. *The European Physical Journal C*, 75(4), Apr 2015. ISSN 1434-6052. doi: 10.1140/epjc/s10052-015-3327-7. URL `http://dx.doi.org/10.1140/epjc/s10052-015-3327-7`.

G. Cowan. *Discovery sensitivity for a counting experiment*, 2012. url: `https://www.pp.rhul.ac.uk/~cowan/stat/medsig/medsigNote.pdf`.

G. Cowan, K. Cranmer, E. Gross, and O. Vitells. Asymptotic formulae for likelihood-based tests of new physics. *The European Physical Journal C*, 71(1554), 2011. doi: 10.1140/epjc/s10052-011-1554-0.

L. Evans and P. Bryant. LHC machine. *Journal of Instrumentation*, 3(08):S08001–S08001, aug 2008. doi: 10.1088/1748-0221/3/08/s08001. URL `https://doi.org/10.1088/1748-0221/3/08/s08001`.

F. Mandl and G. Shaw. *Quantum Field Theory*. John Wiley & Sons Ltd, 2010.

H. Murayama. Supersymmetry phenomenology, Mar 2000. URL `https://arxiv.org/abs/hep-ph/0002232v2`.

A. L. Read. Presentation of search results: the cl$_s$ technique. *Journal of Physics G: Nuclear and Particle Physics*, 28(10):2693–2704, sep 2002. doi: 10.1088/0954-3899/28/10/313. URL `https://doi.org/10.1088/0954-3899/28/10/313`.

The ATLAS Collaboration. The atlas experiment at the cern large hadron collider. *Journal of Instrumentation*, 3(08):S08003–S08003, aug 2008. doi: 10.1088/1748-0221/3/08/s08003. URL `https://doi.org/10.1088/1748-0221/3/08/s08003`.

The ATLAS collaboration. Luminosity determination in pp collisions at $\sqrt{s} = 13$ TeV using the ATLAS detector at the LHC. Technical report, CERN, Geneva, Jun 2019. URL `https://cds.cern.ch/`

record/2677054. All figures including auxiliary figures are available at https://atlas.web.cern.ch/Atlas/GROUPS/PHYSICS/CONFNOTES/ATLAS-CONF-2019-021.

The ATLAS collaboration. Operation of the ATLAS trigger system in run 2. *Journal of Instrumentation*, 15(10):P10004–P10004, oct 2020. doi: 10.1088/1748-0221/15/10/p10004. URL `https://doi.org/10.1088/1748-0221/15/10/p10004`.